Article

# CuO Surfaces and CO$_2$ Activation: A Dispersion-Corrected DFT+U Study

Abhishek Kumar Mishra,[*,†] Alberto Roldan,[‡] and Nora H. de Leeuw[*,†,‡]

†Department of Chemistry, University College London, 20 Gordon Street, London WC1H 0AJ, U.K.

‡School of Chemistry, Cardiff University, Main Building, Park Place, Cardiff CF10 3AT, U.K.

Ⓢ Supporting Information

ABSTRACT: We have used computational methodology based on the density functional theory to describe both copper(I) and copper(II) oxides, followed by the investigation of a number of different low index CuO surfaces. Different magnetic orderings of all the surfaces were studied, and reconstructions of the polar surfaces are proposed. A detailed discussion on stabilities, electronic structure, and magnetic properties is presented. CuO(111) and CuO($\bar{1}$11) were found to have the lowest surface energies, and their planes dominate in the calculated Wulff morphology of the CuO crystal. We next investigated the adsorption of CO$_2$ on the three most exposed CuO surfaces, viz., (111), ($\bar{1}$11), and (011), by exploring various adsorption sites and configurations. We show that the CO$_2$ molecule is activated on the CuO surfaces, with an adsorption energy of −93 kJ/mol on the (011) surface, showing exothermic adsorption, while (111) and ($\bar{1}$11) surfaces show comparatively weak adsorption. The activation of the CO$_2$ molecule is characterized by large structural transformations and significant charge transfer, i.e., forming a negatively charged bent CO$_2^{-\delta}$ species with elongated C−O bonds, which is further confirmed by vibrational analyses showing considerable red shift in the frequencies as a result of the activation.

CO$_2$ activation on CuO surfaces
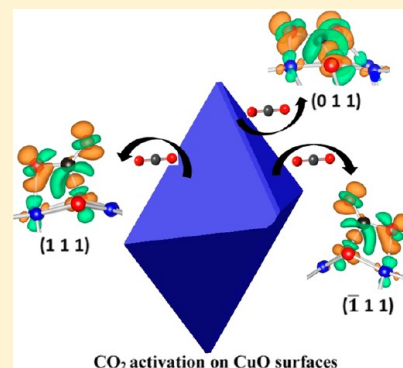
1. INTRODUCTION

Nanostructured transition metal oxides (TMOs) are a class of materials, whose conducting properties range from metallic to semiconducting and which have been developed for a variety of novel advanced functional material applications.[1] In recent years, copper oxides[2,3] have attracted increasing interest in numerous fields, viz., photocatalysis,[4] as energy materials,[5] supercapacitors,[6] batteries,[7] gas sensors,[8] and other applications.[9−12] The physical and chemical properties of nanostructures deviate significantly from their bulk counterpart, and in order to design functional devices based on tailor-made CuO nanostructures, a thorough understanding at the molecular level is necessary. Even though numerous architectures have been prepared by state-of-the-art synthetic methods, a precise understanding of the formation mechanisms of the different morphologies is still challenging.[13]

Carbon dioxide is the primary greenhouse gas responsible for global warming and recent climate changes.[14] In the past few years, copper oxides have been investigated extensively as catalysts in photochemical and electrochemical CO$_2$ reduction.[15−19] However, almost all catalysts, including copper oxides, still suffer from low selectivity and activity. Consequently, we need to understand the factors determining catalytic activity to be able to design for specific applications.[20,21]

It is well-known that transition metal oxides are difficult to model using density functional theory (DFT) with simple local and semilocal functionals.[22] Approximations such as the local

density (LDA)[23] and generalized gradient approximations (GGAs)[24] do not account properly for exchange and correlation effects in transition metal oxides and thus lead to self-interaction errors. Advanced methods such as self-interaction correction (SIC)[25] and the GW approximations (GWA)[26] provide a better description of CuO[27,28] but are very computationally demanding and not appropriate for the large systems required to model surfaces and clusters. However, the DFT+U[29] method, which takes account of the on-site Coulombic repulsion among localized d−d electrons by incorporating an extra energetic penalty for delocalization, has been successful in describing transition metal oxides at relatively low computational cost. DFT+U with an appropriate value of U can accurately describe the CuO structure,[30,31] although both DFT and DFT+U fail in accurately describing the electronic structure of Cu$_2$O.[32] Scanlon et al.[32] suggested a value of U = 5.2 eV, which can closely reproduce the valence band features of Cu$_2$O, whereas Nolan et al.[30] found U = 7 eV as the most accurate value for CuO, which closely reproduces its electronic band gap and magnetic moment. In a recent study by Ekuma et al.,[31] a value of 7.14 eV was suggested as the most suitable value, which gives the closest match to the experimental magnetic moment and band gap values of CuO. As such, computational methods are available to describe both

copper oxides. However, experimentally it is found that copper oxide surfaces consist of mixed Cu_2O and CuO moieties, and there is therefore a need to identify an appropriate value for the U parameter, which can describe adequately both CuO and Cu_2O in terms of experimental properties. In the present work, we aim to determine such a U parameter, through systematic investigation of structural, magnetic, and electronic properties of both the copper oxides.

Control of the shape and structure of copper oxide nanocrystals has recently attracted significant interest, and different morphological structures have been synthesized for various applications.[13,33−35] Among their different properties, including electrical applications and in gas sensing, the catalytic properties are strongly influenced by the morphological surface structures. In the present work, we provide a detailed first-principles-based electronic structure study of different low index surfaces of CuO, including the resulting calculated equilibrium morphology, and discuss the stability of these nonpolar surfaces through analyzing their structural, electronic, and magnetic properties. Electronic structure engineering is an effective tool to tailor catalytic surfaces by elucidating the relationship between atomic-scale properties and the macroscopic functionality,[36] and as the adsorption of molecules on a catalyst surface is the first step in their activation and conversion, we have investigated CO_2 adsorption on the different surfaces appearing in the CuO morphology by elucidating structural, vibrational, and electronic properties of different adsorbed geometries. Catalytic processes are highly complex in nature, occurring in a multicomponent environment, and are influenced by various environmental parameters: temperature, pressure, and electrode potential. Nevertheless, DFT calculations at 0 K, as presented in this paper, provide mechanistic insight into CO_2 activation on CuO surfaces, and this fundamental understanding will still be relevant for applications at elevated temperatures.

2. COMPUTATIONAL METHODOLOGY

Spin-polarized calculations were performed using the Vienna Ab-initio Simulation Package (VASP) with a plane-wave basis set.[37−40] We have employed DFT+U[29] methodology with the PBE[25,41] exchange-correlation functional and the formalism of Dudarev et al.[29] The U_{eff} value is selected for the localized 3d electrons of Cu, where $U_{eff} = U − J$, i.e., the difference between the Coulomb U and exchange J parameters. The Brillouin zone was sampled using a $9 \times 9 \times 9$ Monkhorst−Pack[42] k-point mesh for the primitive cells of both Cu_2O and CuO. Such dense grids and a truncation kinetic energy of 450 eV for the plane waves ensured an accurate description of properties that are influenced by sharp features in the density of states. A total energy convergence better than 10^{-5} eV per unit cell was required, and the interatomic forces were minimized to 0.01 eV/Å for the structural relaxations. Magnetic moments were calculated using the code developed by Henkelman and co-workers.[43,44]

The different CuO surfaces were obtained by the METADISE code,[45] providing all possible nonpolar surface terminations. At the base of the surface simulation cell, two layers of atoms were fixed at their relaxed bulk positions to simulate the bulk phase of the crystal. Above these two layers, the surface is represented by two layers of atoms whose positions are allowed to change freely during optimization. In each case, the vacuum region above the surface was at least 15 Å, i.e., large enough to avoid interactions between the periodic

slabs. Different slab and vacuum thicknesses as well as numbers of relaxed layers were tested until convergence within 1 meV per atom was achieved. We sampled the (1×1) surface cells with a $5 \times 5 \times 1$ Monkhorst−Pack[42] k-point mesh.

The surface energies of the relaxed slabs were obtained using a combination of calculations for the relaxed and unrelaxed surfaces. After surface relaxation, the top and bottom surfaces are not equivalent, and therefore we also need to consider the unrelaxed surface energy (γ_u) when we calculate the final surface energy of the relaxed surface.

The unrelaxed surface energy is the surface energy before any surface optimization and is calculated as

$$\gamma_u = \frac{E_{slab,u} - nE_{bulk}}{2A} \tag{1}$$

where $E_{slab,u}$ is the energy of the unrelaxed slab; nE_{bulk} is the energy of an equal number of bulk atoms; and A is the surface area of one side of the slab. Using this value, it is then possible to calculate the relaxed surface energy (γ_r) from the total energy of the relaxed slab.

The relaxed surface energy, γ_r, is given by

$$\gamma_r = \frac{E_{slab,r} - nE_{bulk}}{A} - \gamma_u \tag{2}$$

where $E_{slab,r}$ is the energy of the relaxed slab.

Electronic density-of-states (DOS) were calculated using a higher $9 \times 9 \times 1$ Monkhorst−Pack[42] k-point mesh with a tetrahedron smearing parameter of 0.2 eV and a self-consistent-field (SCF) convergence criterion of 1×10^{-6} eV per unit cell (a (1×1) simulation slab consisting of 16 Cu and 16 O atoms) for all the surfaces. The equilibrium morphology of a CuO particle (ignoring higher Miller indices) was constructed using Wulff's method,[46] in which the distance to a given surface from the center of the particle is proportional to the surface energy.

We modeled the CO_2 adsorption by taking into account the long-range dispersion forces, which is essential for the accurate description of the interaction between CO_2 and CuO surfaces, where we have used the correction according to the Grimme method[47] for the long-range interactions (DFT-D2). While modeling the interactions of the CO_2 adsorbate with the CuO surface slabs, the atoms of the adsorbate and the two topmost layers of the slab were allowed to relax unconstrainedly until residual forces on all atoms reached 0.01 eV/Å. In order to avoid periodic interactions between neighboring CO_2 molecules, we have studied the CO_2 adsorption on a (2×2) supercell in all the surfaces. Symmetry constraints were not included in the structural optimization; in particular, the CO_2 molecule was free to move in all directions to reorient itself in order to find its minimum energy adsorption structure.

The adsorption energy per molecule was calculated from the relation

$$E_{ads} = E_{surf+mol} - (E_{surf} + E_{mol}) \tag{3}$$

where $E_{surf+mol}$ is the total energy of the adsorbate−substrate system; E_{surf} is the energy of the naked surface slab; and E_{mol} is the energy of the isolated CO_2 molecule. Within this definition, a negative adsorption energy indicates an exothermic process.

The isolated molecule was modeled in the center of a broken symmetry cell with lattice constants of 20 Å, sampling only the Gamma-point of the Brillouin zone with the same accuracy parameters described for the surfaces. A Bader analysis was carried out, using the code developed by Henkelman and co-

workers,[43,44] to quantify the charge transfer between the surfaces and CO_2 moiety.

3. RESULTS AND DISCUSSION

3.1. Determination of a Single Hubbard U Parameter for CuO and Cu₂O.
Copper oxide exists as a compound
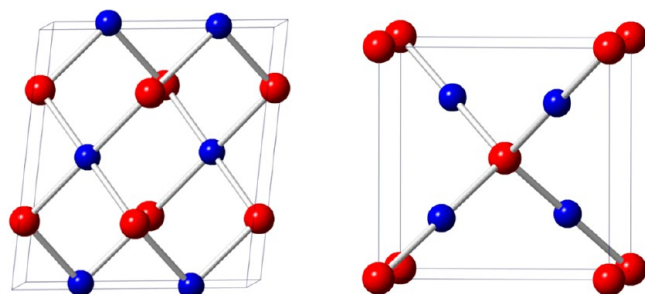
Figure 1. Representation of CuO (left) and Cu₂O (right) bulk structures. Blue and red balls indicate Cu and O atoms, respectively.

semiconductor in two different metal oxidation states, Cu(I) and Cu(II); Cu₂O is a Bloch semiconductor, while CuO is usually regarded as a Mott or charge-transfer insulator driven by strong electron correlation. These two compounds have energy band gaps in the ranges 2.2–2.4 eV[48−50] and 1.4−1.7 eV,[50−53] respectively. Cuprous oxide (Cu₂O) has a cubic structure (space group: $Pn3m$) with a lattice parameter of 4.270 Å,[54] while CuO has a monoclinic crystal structure with $C2/c$ symmetry,[55] as shown in Figure 1. Experimentally, it is known that CuO has a local magnetic moment per formula unit of 0.65−0.69 μ_B.[56−58] However, due to nonzero self-interaction errors of DFT and delocalization of electrons in such materials, pure DFT provides an incorrect description of both CuO and Cu₂O.

We first modeled the CuO structure by considering the bulk unit cell. We systematically varied U_{eff} in intervals of 1 eV up to 9 eV and compared the lattice parameters, magnetic moment, and band gap values with the experimental values (Table 1). As expected, at U_{eff} = 0 eV there is no band gap, and d-states cross the Fermi level (Figure 2) with nonmagnetic states on the Cu atoms. We note that an increase in the U_{eff} value causes both the band gap (E_g) and magnetic moment (m_s) to increase (Figure 3). At U_{eff} = 3 eV a band gap opens in the system with a shift of d-states beyond the Fermi energy, and at U_{eff} = 7 eV, we obtain a band gap (E_g) and a magnetic moment (m_s) of 1.53 eV and 0.67 μ_B, respectively, in good agreement with the experimental values. We have plotted the variation of E_g and
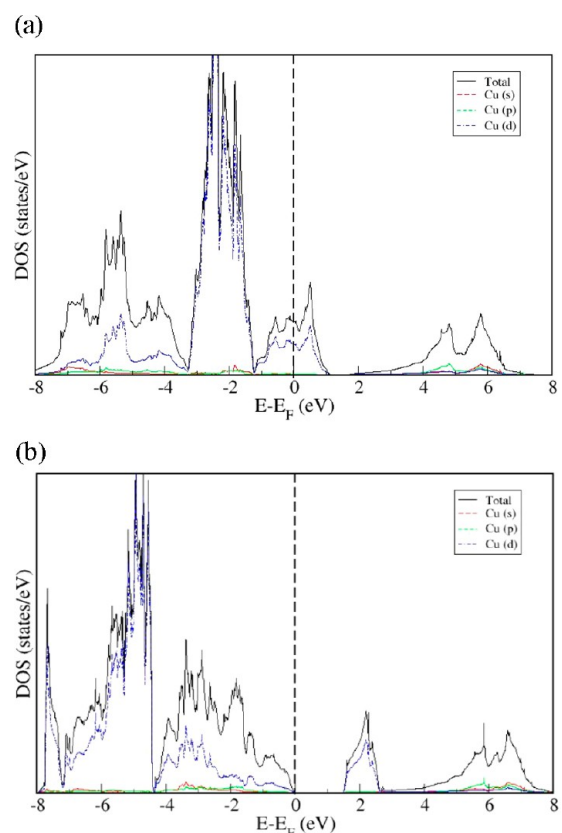

Figure 2. (a) Density of states of CuO with DFT and (b) with DFT+U (U_{eff} = 7 eV). Solid black line indicates the total DOS, and dashed lines are the projected DOS over d-orbitals (blue color), p-orbitals (green color), and s-orbitals (red color). Perpendicular dashed line shows the Fermi energy.

m_s as a function of U_{eff} (Figure 3) showing that with further increase in U_{eff} beyond 7 eV both magnetic moment and band gap values start deviating from their experimental values. We note that U_{eff} = 7 eV not only reproduces an accurate band gap and magnetic moment for CuO but also results in a good match of structural parameters.[57] Our results are in reasonable agreement with earlier work by Nolan et al.,[30] where they studied the effect of the U_{eff} value on Cu−O distances, magnetic moment, and band gap. As already mentioned in the Introduction section, by utilizing experimental lattice parameters Ekuma et al.[31] recently suggested a U_{eff} value of 7.14 eV using PBE+U methodology; we repeated our calculations with this U_{eff} value, but no significant changes were observed in any of the parameters.

Table 1. Summary of Calculated Lattice Parameters (a, b, c, and β), Cu−O Distances ($d_{Cu−O}$), O−O Distances ($d_{O−O}$), Band Gap (E_g), and Magnetic Moment (m_s) for CuO Bulk at Different U_{eff} Values, Compared to the Experimental Values

U_{eff} (eV)	a (Å)	b (Å)	c (Å)	β (deg)	$d_{Cu−O}$ (Å)	$d_{O−O}$ (Å)	E_g (eV)	m_s (μ_B)
0	4.597	3.537	5.168	96.19	1.928	2.599	-	0
3	4.657	3.506	5.152	98.06	1.966	2.613	0.44	0.55
4	4.660	3.502	5.158	98.02	1.965	2.615	0.68	0.58
5	4.665	3.498	5.155	98.12	1.965	2.618	0.95	0.61
6	4.673	3.493	5.156	98.22	1.966	2.620	1.23	0.64
7	4.688	3.481	5.156	98.26	1.966	2.623	1.53	0.67
8	4.692	3.481	5.156	98.52	1.967	2.627	1.86	0.70
9	4.708	3.468	5.159	98.57	1.967	2.631	2.21	0.73
exptl[48−50,56−58]	4.6837	3.4226	5.1288	99.54	1.951	2.625	1.4−1.7	0.65−0.69

(a)

(b)
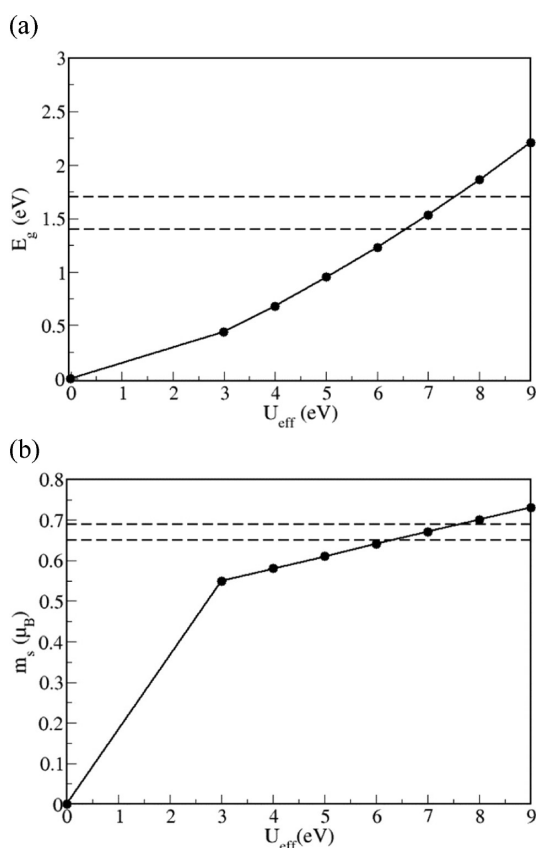
Figure 3. (a) Variation of band gap (E_g) and (b) magnetic moment (m_s) as a function of U_{eff} value in CuO. Horizontal dashed lines indicate range of experimental values.

Table 2. Summary of Calculated Lattice Parameters (a_0), Cu−O Distances (d_{Cu-O}), O−O Distances (d_{O-O}), and Cu−Cu Distances (d_{Cu-Cu}) for Cu_2O Bulk at Different U_{eff} Values, Compared to the Experimental Values

structural parameters	exptl[59]	U_{eff} (eV)				
		0	5	6	7	8
a_0 (Å)	4.2696	4.299	4.277	4.275	4.272	4.269
d_{Cu-O} (Å)	1.84	1.862	1.852	1.851	1.850	1.849
d_{O-O} (Å)	3.68	3.723	3.704	3.702	3.699	3.698
d_{Cu-Cu} (Å)	3.02	3.040	3.024	3.024	3.021	3.019

Cu_2O crystallizes in a simple cubic structure which can be viewed as two sublattices, a face-centered cubic (fcc) sublattice of copper cations and a body-centered cubic (bcc) sublattice of oxygen anions, as shown in Figure 1. The oxygen atoms occupy tetrahedral interstitial positions relative to the copper sublattice, whereas copper is linearly coordinated by two neighboring oxygens. Here, it is known that both DFT and DFT+U fail to predict an accurate band structure for Cu_2O.[30,59] Considering different values of U_{eff}, we found lattice parameter and band gap values of 4.30 Å and 0.45 eV, respectively, for U_{eff} = 0 eV. From the projected DOS of s, p, and d states in the total DOS of Cu_2O (Figure S1) we note significant 4s states near the Fermi level as well as the 3d states. As we apply U_{eff} only to d states we see that the band gap value increases from 0.45 to 0.89 eV at U_{eff} = 7 eV, although it is still underestimated due to its Bloch semiconductor character.[48−50] At this U_{eff} value, we found the lattice parameter to be 4.270 Å, which is very close to the experimental value of 4.2696 Å.[59] Other structural parameters are also found to be in close agreement with the experimental values, as shown in Table 2. Our U_{eff} varies slightly from recent work by Isseroff et al.,[60] in which they mention that U_{eff} = 6 eV gives better agreement with the lattice parameter of Cu_2O. Although the Hubbard correction U_{eff} does not modify the E_g substantially for Cu_2O, a value of U_{eff} = 7 eV results in the accurate reproduction of the structural parameters of the Cu(II) oxide.

3.2. CuO Surfaces: Reconstruction, Electronic, and Magnetic Properties. Tasker[61] considered ionic crystal surfaces as stacks of planes, where three possibilities (type I, II, and III) can arise. In a type I surface, each plane has overall zero charge because it is composed of anions and cations in stoichiometric ratio which also makes the surface nonpolar. In a type II surface, the symmetrical stacking of three charged planes cancels out the opposite dipole moment, so in type I and II no reconstruction of the surface is needed because the repeat unit has no net dipole perpendicular to the surface. However, in type III surfaces, alternating charged planes stack in a sequence that produces an overall dipole moment perpendicularly to the surface, which means that the surface energy will diverge with the size of the slab. Furthermore, polar surfaces are not stable experimentally.[63] However, this dipole can be canceled by reconstruction of the surface through moving half of the ions with the same charge from the top to the bottom of the simulation slab. This dipole method also guarantees that the surface does not generate an electrical field within the crystal, and therefore the potential felt at each ion site reaches the
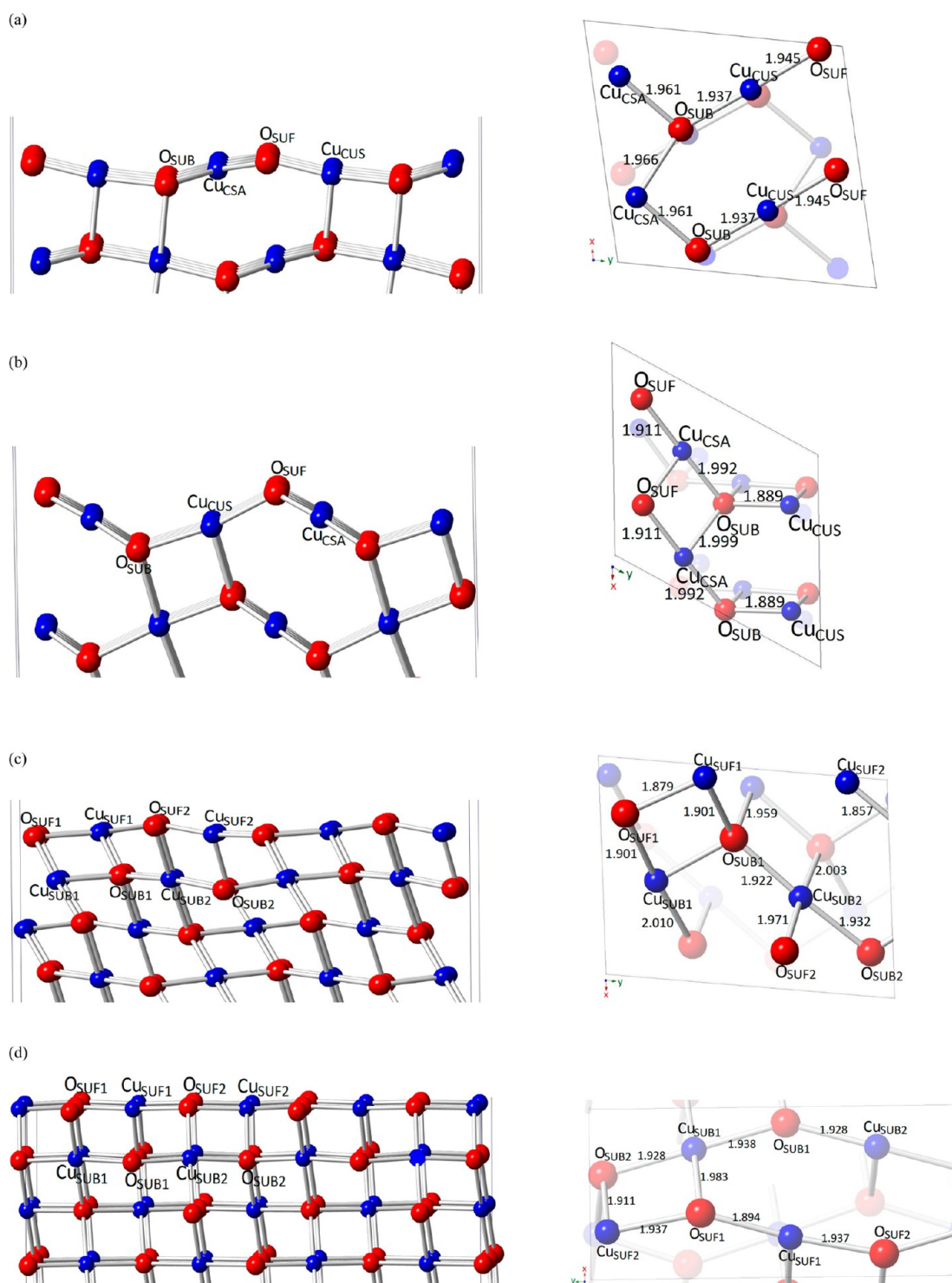
Table 3. Surface Energies (γ), Work Functions (Φ), and Magnetic Moments (m_S) of Top Surface Cu Atoms and Band-Gap (E_g) Values for Different CuO Surfaces[a]

surface	γ (J/m^2)	Φ (eV)	m_S (μ_B)	E_g (eV)
(111)	0.75	5.24	0.68 (Cu_{CSA}), 0.64 (Cu_{CUS})	0.84
($\bar{1}$11)	0.89	5.79	0.66 (Cu_{CSA}), 0.62 (Cu_{CUS})	0.50
(011)	0.94	5.20	0.67 (Cu_{SUF1}), 0.67 (Cu_{SUF2})	0.94
(101)	1.17	5.08	0.67 (Cu_{SUF1}), 0.67(Cu_{SUF2})	0.97
(110):Cu	1.00	4.28	0.59 (Cu_{SUF})	0.00
(110):Cu−O and (110):O	1.37	-	-	-
(010):O	1.35	5.92	0.63 (Cu_{SUF1}), 0.63 (Cu_{SUF2})	0.49
(010):Cu	1.62	-	-	-
(100):Cu	1.83	-	-	-
(100):O	1.68	6.62	0.60 (Cu_{SUF1}), 0.70 (Cu_{SUF2})	0.22

[a]We have calculated workfunction, magnetic moments, and band gap values only for the most stable surface terminations.

Figure 4. (a) CuO(111), (b) ($\bar{1}$11), (c) (011), and (d) (101) surface structures after relaxations. Left panel figures show the side view of the (2 × 2) supercell, while right panel figures show the top view of the (1 × 1) cell. We have shown (2 × 2) supercell structures with top 2-layers only for a clear visualization of bonding and atomic arrangements in side view figures. Bond length values are in Angstroms. Blue and red balls indicate Cu and O atoms, respectively.

constant bulk value, a condition that is not necessarily satisfied by the alternative electron-counting model.[62]

Similar to work of Hu et al.,[63] we have focused our attention on seven different low index surfaces of CuO, viz., (111), ($\bar{1}$11), (110), (011), (101), (010), and (100), and investigated three different possible magnetic orderings in the surfaces, i.e., bulk-like, line-by-line, or layer-by-layer (Figure S2). We note that

among the seven low-index surfaces the (110), (010), and (100) are Tasker type III surfaces, and hence reconstruction is required to obtain realistic nonpolar stoichiometric surfaces.

In the following sections, we discuss the structures of the different surfaces, giving details of the different surface reconstructions and stabilities with respect to magnetic ordering. We also discuss the band gap and changes in
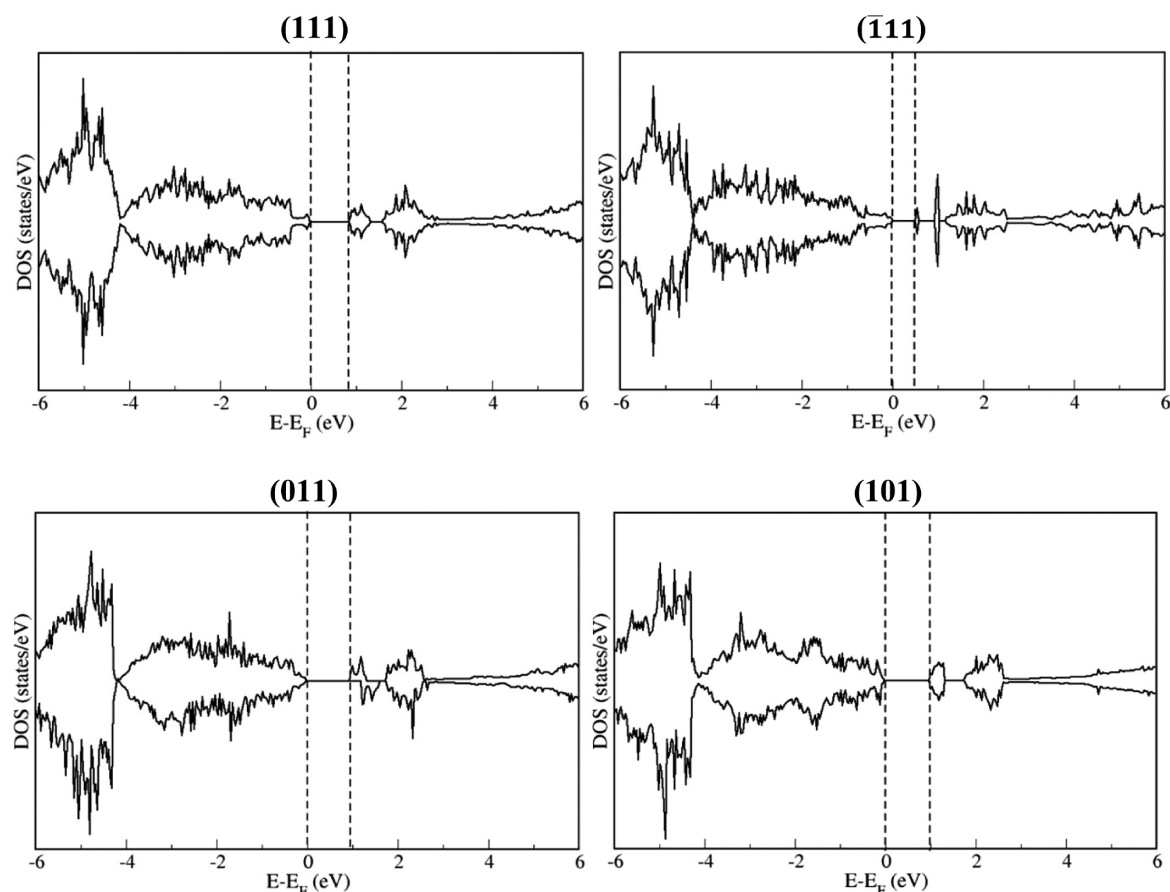
Figure 5. Electronic density-of-states (DOS) of CuO(111), ($\bar{1}$11), (011), and (101) surfaces with Fermi level set to zero. Double dashed lines show the band gap.

magnetic moment of the surface atoms in the various surfaces. Table 3 lists the surface energies of the surfaces, as well as the magnetic moments of top layer atoms, work functions, and band gaps.

CuO(111) Surface. CuO(111) is the most stable surface with a calculated surface energy of 0.76 J/m^2. The top layer consists of 3- and 4-coordinated Cu and O atoms (Figure 4). 3-coordinated O atoms (O_{SUF}) are the most exposed atoms, connected to one 3-coordinated (coordinatively unsaturated $-Cu_{CUS}$) and two 4-coordinated (coordinatively saturated $-Cu_{CSA}$) Cu atoms as shown in Figure 4. Subsurface oxygen atoms (O_{SUB}) are 4-coordinated, connected to two Cu_{CSA} atoms on two sides, one Cu_{CUS} atom, and one Cu atom in the second layer. After relaxation, we note that the subsurface oxygen, O_{SUB}, moves up to increase the vertical Cu−O_{SUB} bond distance from 1.958 to 2.032 Å, while the Cu_{CUS}−O_{SUF} and Cu_{CSA}−O_{SUB} bond lengths shrink from 1.966 to 1.852 Å and 1.922 Å, respectively.

Among three possible magnetic orderings, we found that CuO(111) is most stable in the bulk-like magnetic ordering, while line-by-line and layer-by-layer ordered structures lead to less stable surface energies by 0.01 and 0.13 J/m^2, respectively. However, the negligible small difference in surface energies of bulk-like and line-by-line magnetically ordered surfaces suggests the co-existence of both these magnetic orderings. The work function calculated for this surface is found to be 5.24 eV, which matches the experimental value of 5.23 eV[64] and is in better agreement than earlier work.[63] The calculated electronic density of states (DOS) (Figure 5) shows that the band gap of

this surface is reduced to 0.84 eV from a bulk value of 1.56 eV. Investigation of the magnetic moments of the surface atoms reveals that the 4-coordinated Cu atoms possess magnetic moments of 0.68 μ_B which is close to their bulk value of 0.67 μ_B, although the magnetic moment reduces to 0.64 μ_B for the 3-coordinated Cu surface atoms. Magnetic moments of Cu atoms in the second and third layers are found to vary from 0.66 μ_B to 0.68 μ_B. We note that the surface O atoms acquire 0.10 μ_B magnetic moment, but they are antiparallel to each other and hence do not result in any effective contribution to the total magnetic moment of the system.

CuO($\bar{1}$11) Surface. The CuO($\bar{1}$11) is the second most stable surface with a calculated surface energy of 0.89 J/m^2. Similar to the CuO(111) surface, we note that the bulk-like magnetic ordering is preferred over line-by-line and layer-by-layer orderings. However, the surface energies with the other two magnetic orderings are very similar, with the surface energy increasing by only 0.03 and 0.02 J/m^2 for line-by-line and layer-by-layer orderings, respectively. Again, this small difference in surface energies suggests the possible coexistence of all three magnetically ordered structures, which is in accordance with earlier findings of Hu et al.[63] The work function calculated for the CuO($\bar{1}$11) surface is 5.79 eV, i.e., larger than that of the CuO(111) surface.

Similarly to the CuO(111) surface, upon relaxation, subsurface oxygen, O_{SUB}, moves up into the surface, thereby increasing the vertical bond distance O_{SUB}−Cu from 1.966 to 2.026 Å (Figure 4). Bond lengths of Cu_{CUS}−O_{SUF} and Cu_{CUS}−O_{SUB} shrink from 1.958 to 1.796 Å and 1.889 Å, respectively.
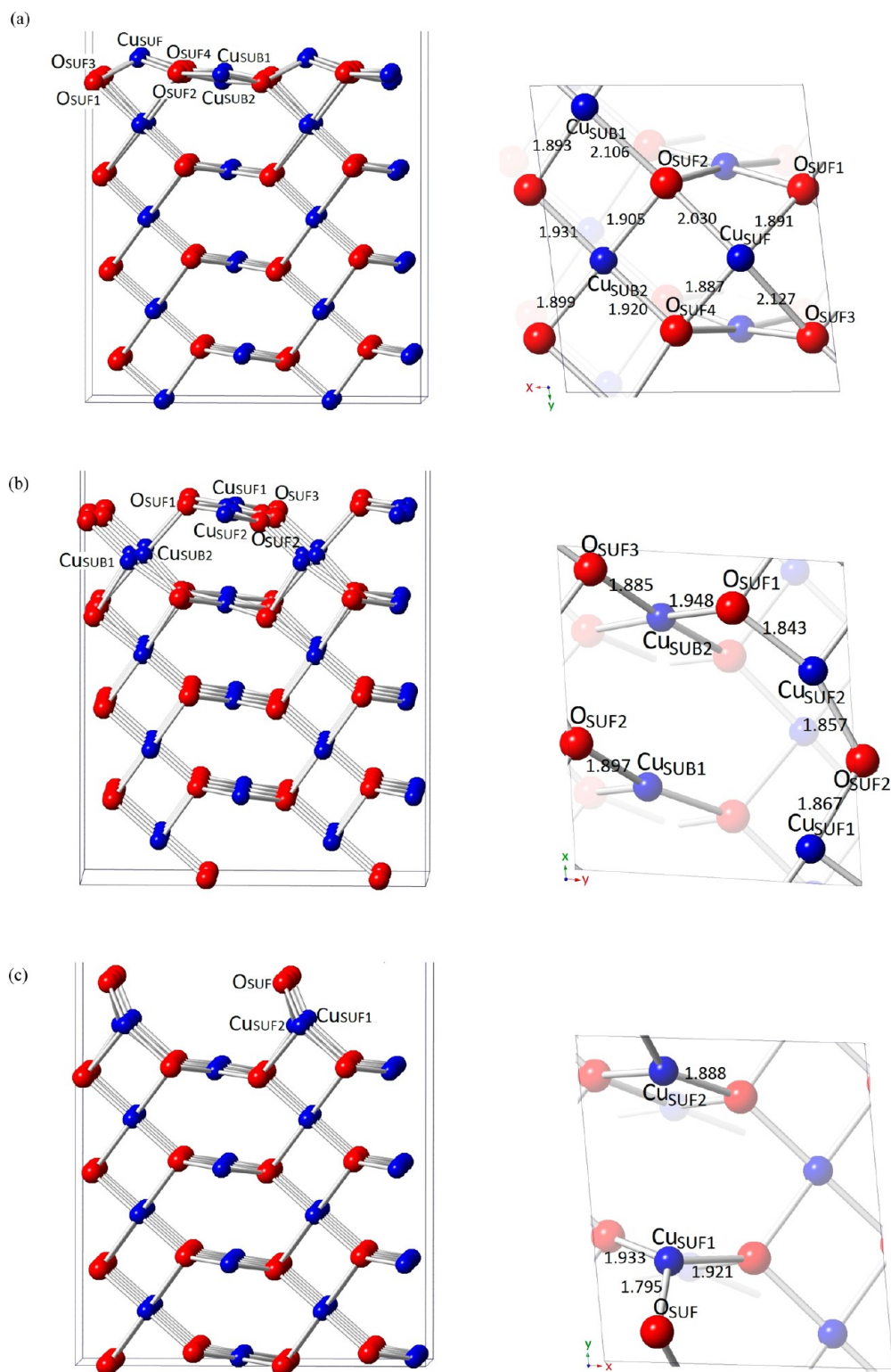
Figure 6. (a) CuO(110):Cu, (b) CuO(110):Cu−O, and (c) CuO(110):O surface structures after relaxation. Left panel shows the side view of the (2 × 2) supercell, while the top view of a (1 × 1) cell is shown in the right panel. In side view figures, we have shown a (2 × 2) supercell for a clear visualization of bonding and atomic arrangements. Bond length values are in Angstroms. Blue and red balls indicate Cu and O atoms, respectively.

The band gap for this surface reduces to 0.50 eV, as shown in Figure 5. Similar to the CuO(111) surface, the magnetic moments of the 3-coordinated surface copper atoms change to 0.62 μ_B, while those of the 4-coordinated copper atoms (0.66 μ_B) remain close to their bulk values (0.67 μ_B). The surface

oxygen atoms gain small antiparallel magnetic moments ∼0.12 μ_B.

CuO(011) Surface. The CuO(011) surface is the third most stable surface with a surface energy of 0.94 J/m². The work function calculated for this surface is 5.20 eV which is close to that of the most stable CuO(111) surface. The surface energies
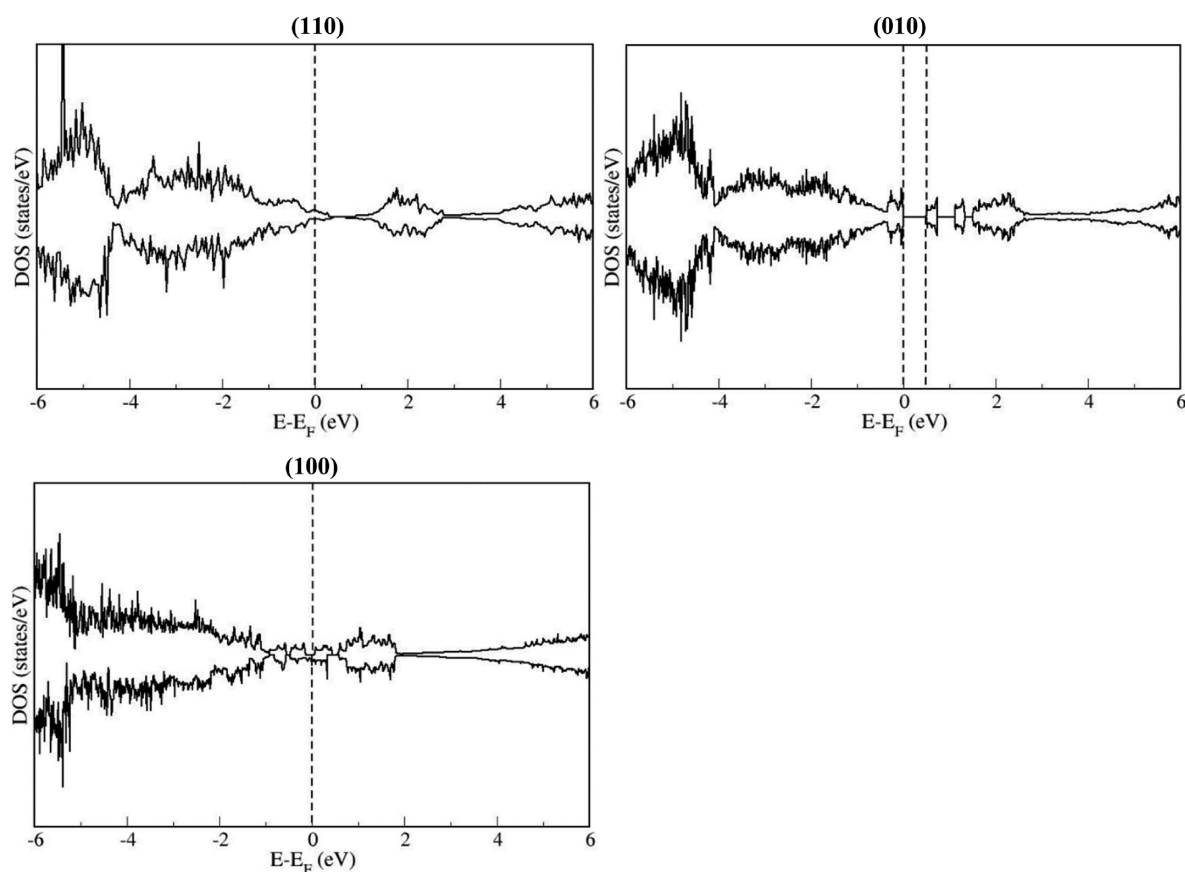
Figure 7. Electronic density-of-states (DOS) of the most stable terminations of the CuO(110), (010), and (100) surfaces with Fermi level set to zero. Dashed lines show the Fermi level and band gaps.

of three different magnetically ordered structures differ by only 0.006 J/m^2, with bulk-like magnetic ordering as marginally the most stable magnetic ordering. The CuO(011) surface consists of 3-coordinated O and Cu atoms, connected in a zigzag line as shown in Figure 4. Surface oxygens, O_{SUF}, are the most exposed atoms bonded to two 3-coordinated Cu atoms (Cu$_{SUF1}$ and Cu$_{SUF2}$) at the top and one 3-coordinated Cu atom (Cu$_{SUB}$) vertically underneath in the z-direction. Similarly, Cu$_{SUF1}$ and Cu$_{SUF2}$ atoms are bonded to two O atoms, O_{SUF1} and O_{SUF2}, in two directions and one O_{SUB} atom below. After relaxation, both surface oxygen atoms, O_{SUF1} and O_{SUF2}, move up, thereby increasing vertical bond distances, $d_{OSUF1-CuSUB1}$ and $d_{OSUF2-CuSUB2}$, to 2.023 and 1.971 Å from 1.958 and 1.966 Å, respectively. Bond lengths in the top layer, viz., $d_{OSUF1-CuSUF2}$ and $d_{OSUF2-CuSUF2}$, shrink to 1.857 and 1.877 Å, respectively, from 1.966 Å, whereas bond distances $d_{OSUF1-CuSUF1}$ and $d_{OSUF2-CuSUF1}$ shrink to 1.879 and 1.834 Å, respectively, from 1.958 Å. Bond distances between Cu atoms at the top (Cu$_{SUF1}$ and Cu$_{SUF2}$) and O atoms below (O_{SUB1} and O_{SUB2}), i.e., $d_{CuSUF1-OSUB1}$ and $d_{CuSUF2-OSUB2}$, also shorten to 1.901 and 1.918 Å from 1.966 and 1.958 Å, respectively.

Electronic DOS of the CuO(011) surface (Figure 5) show that this surface is a semiconductor with a 0.94 eV band gap for spin-up, while for spin-down the band gap increases to 1.18 eV. We note that the top surface copper atoms, Cu$_{SUF1}$ and Cu$_{SUF2}$, as well as subsurface copper atoms, Cu$_{SUB1}$ and Cu$_{SUB2}$, maintain their bulk magnetic moments with 0.67 μ_B and 0.66 μ_B values on each, respectively, while a small magnetic moment of ±0.08 μ_B is induced on the surface oxygen atoms.

CuO(101) Surface. The surface energy of the CuO(101) surface is relatively high at 1.17 J/m^2, while the value of the work function is low at 5.08 eV. Line-by-line magnetic ordering is marginally preferred for this surface over bulk-like and layer-by-layer magnetic orderings, as their surface energies are higher, by 0.01 and 0.06 J/m^2 for the bulk-like and layer-by-layer magnetic orderings, respectively. The CuO(101) surface consists of 3-coordinated copper (Cu$_{SUF}$) and oxygen (O_{SUF}) atoms in the top layer, as shown in Figure 4. These Cu$_{SUF}$ atoms are connected to two oxygen atoms on two sides and one oxygen atom below, and similarly, O_{SUF} atoms are bonded to two oxygen atoms on two sides and one oxygen atom below. After relaxation, we note that the bond distance $d_{OSUF-CuSUB}$ changes to 1.983 from 1.958 Å as these oxygen atoms move upward, while the Cu$_{SUF}$–O_{SUB} bond, shrinks from 1.958 to 1.911 Å. Cu–O bond distances in the top layer also shrink as $d_{OSUF1-CuSUF1}$ and $d_{OSUF1-CuSUF2}$ change to 1.937 and 1.894 Å, respectively from 1.966 Å in the unrelaxed surface.

From the electronic DOS (Figure 5) we see that the band gap of the CuO(101) surface is 0.97 eV. Similarly to the CuO(011) surface, here copper atoms Cu$_{SUF1}$ and Cu$_{SUF2}$ and subsurface Cu$_{SUB1}$ and Cu$_{SUB2}$ possess magnetic moments of 0.67 μ_B and 0.66 μ_B, respectively. Surface oxygens (O_{SUF}) and subsurface oxygens (O_{SUB}) gain small magnetic moments of 0.03 μ_B and 0.09 μ_B, respectively.

CuO(110) Surface. The CuO(110) surface is a Tasker type III surface and hence needs reconstruction to make it nonpolar. One possible reconstructed termination, (110):Cu, is shown in Figure 6a (unrelaxed structure is given in SI as Figure S3a), where we have moved one Cu atom from the top to the bottom
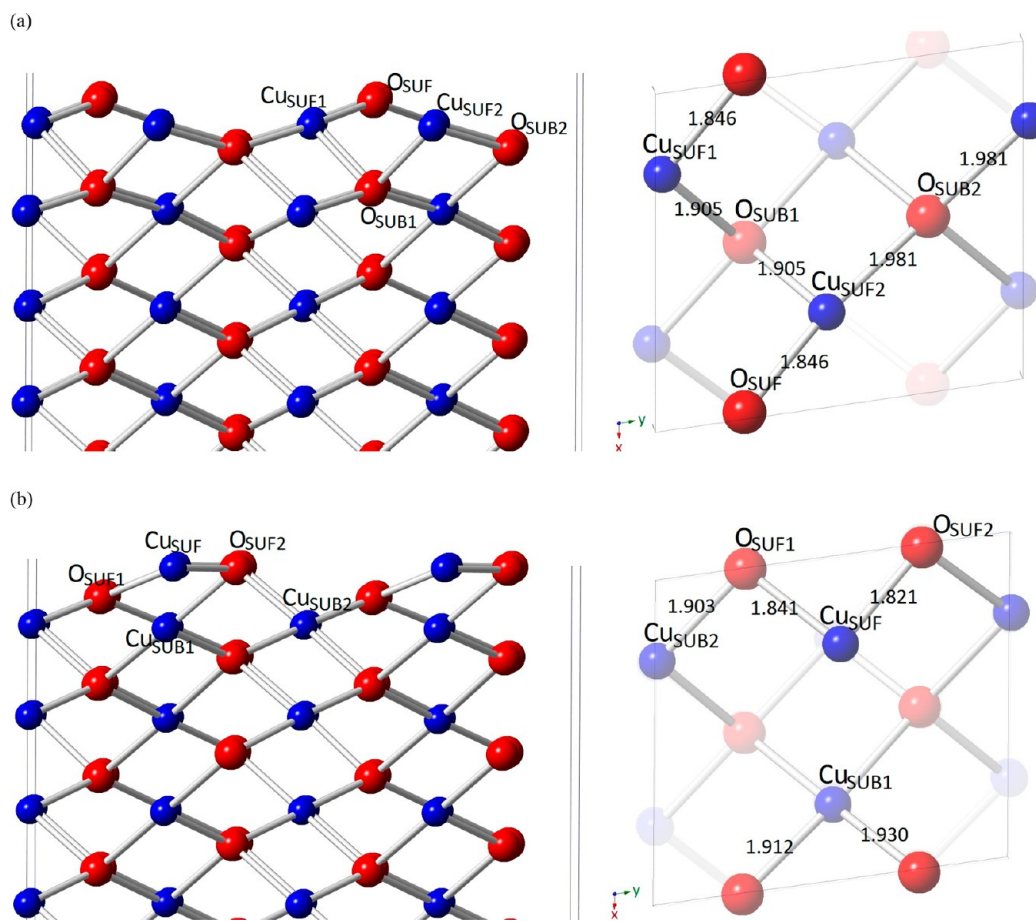
Figure 8. (a) CuO(010):O and (b) CuO(010):Cu surface structures after relaxation. Left panel shows the side view of the (2×2) supercell, while the top view of (1×1) cells is shown in the right panel. We have shown (2×2) supercell structures with the top two layers only for a clear visualization of bonding and atomic arrangements in side view figures. Bond length values are in Angstroms. Blue and red balls indicate Cu and O atoms, respectively.

of the surface slab. Cu atoms at the top connect to oxygen below to create O–Cu–O moieties. After relaxation we observe that these top Cu atoms (Cu_{SUF}), which were only 2-coordinated as a result of the reconstruction, have moved down to bond to four oxygen atoms (O_{SUF1}, O_{SUF2}, O_{SUF3}, O_{SUF4}), thus becoming 4-coordinated. The bond lengths of these Cu_{SUF}–O_{SUF} bonds vary from 1.887 to 2.127 Å. Subsurface copper atoms, Cu_{SUB1} and Cu_{SUB2}, are also 4-coordinated, connected to oxygens with bond lengths varying from 1.888 to 2.115 Å. The calculated surface energy for this termination is 1.00 J/m^2.

In a second reconstruction, (110):Cu–O (Figure 6b, Figure S3b), we have moved one oxygen atom from the top to the bottom of the slab, resulting in an asymmetrical surface along the z-axis with complementary top and bottom layers. As a result of this reconstruction, surface (Cu_{SUF1}, Cu_{SUF2}) and one of the subsurface (Cu_{SUB1}) copper atoms become 3-coordinated because of the missing oxygen atom at the top. After relaxation, we note that subsurface Cu (Cu_{SUB2}) moves upward to bond more strongly with surface oxygen atoms, with the bond length for Cu_{SUB2}–O_{SUF1} shortening to 1.948 Å from 1.958 Å. Cu–O bond lengths in the top layer, viz., O_{SUF1}–Cu_{SUF1} and O_{SUF1}–Cu_{SUF2}, are found to be 1.845 and 1.843 Å, respectively, while O_{SUF2}–Cu_{SUF1} and O_{SUF2}–Cu_{SUF2} bond lengths are 1.867 and 1.857 Å, respectively. Vertical bonds lengths between top layer oxygen atoms and subsurface Cu

atoms, viz., O_{SUF2}–Cu_{SUB1} and O_{SUF3}–Cu_{SUB2}, are found to be 1.885 and 1.897 Å, respectively.

In a third surface reconstruction, (110):O, the top and bottom layers are reversed with respect to termination B (Figure 6c, Figure S3c). At the top we now have one oxygen atom (O_{SUF}) connected to a copper atom (Cu_{SUF}) underneath, which is further connected to two oxygen atoms below. After relaxation these top O atoms bend down to bond to a further Cu atom, thus becoming doubly coordinated, with bond lengths O_{SUF}–Cu_{SUF1} and O_{SUF}–Cu_{SUF2} of 1.792 and 1.795 Å, respectively. As (110):Cu–O and (110):O terminations have complementary top and bottom layers, their surface energy is calculated as the average of the surface energies of these two terminations and found to be 1.37 J/m^2.

Another reconstruction can be obtained by moving half of the Cu and O atoms from a top O–Cu–O moiety to the bottom. However, this reconstruction relaxed into an unrealistic configuration with a very high surface energy (1.83 J/m^2), indicating that this configuration is not likely to appear under standard experimental conditions.

We note that bulk-like magnetic ordering is preferred in the (110) surface as the surface energy increases by 0.09 and 0.02 J/m^2 for layer-by-layer and line-by-line magnetic orderings, respectively, for the most stable, (110):Cu, termination. We have calculated the electronic DOS for this termination and found the surface to be metallic with states crossing at the
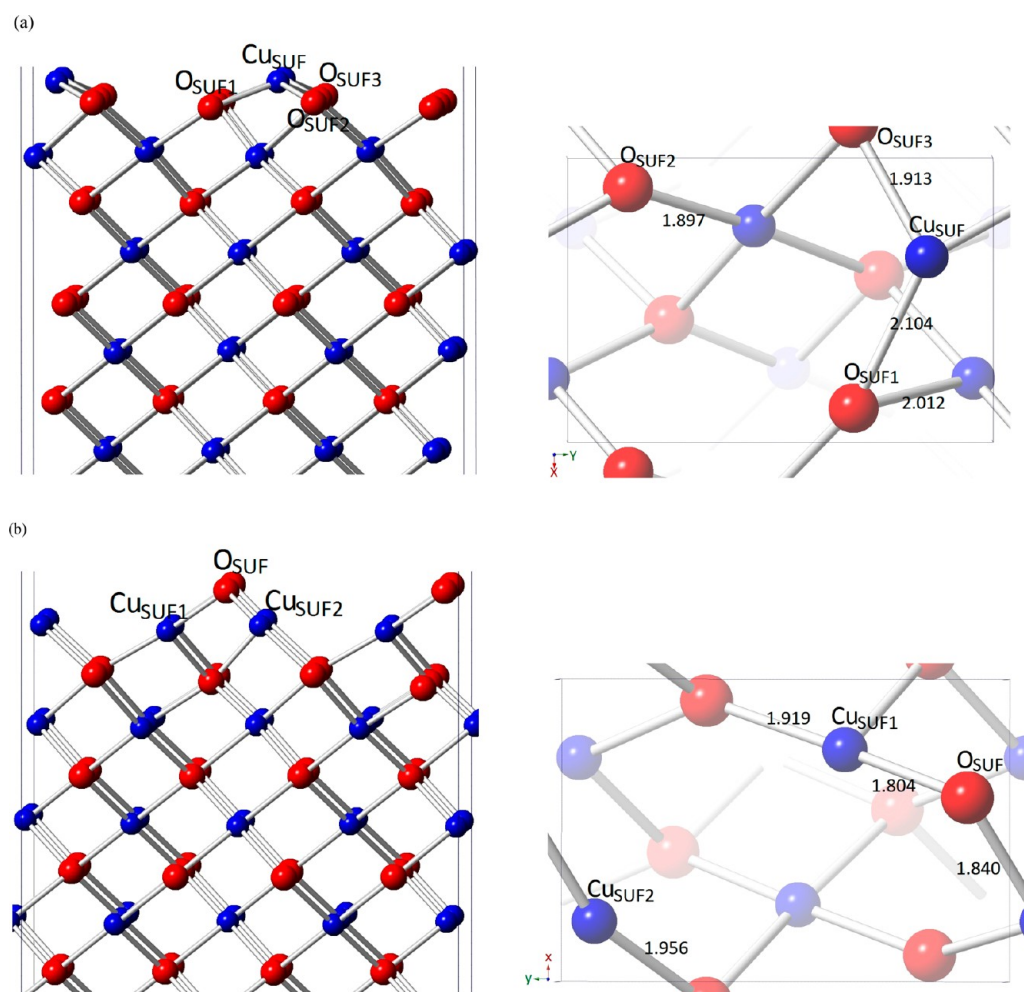
Figure 9. (a) CuO(100):Cu and (b) CuO(100):O surface structures after relaxation. Left panel shows the side view of the (2 × 2) supercell, while the top view of the (1 × 1) cells is shown in the right panel. We have shown (2 × 2) supercell structures with the top 2 layers only for a clear visualization of bonding and atomic arrangements in side view figures. Bond length values are in Angstroms. Blue and red balls indicate Cu and O atoms, respectively.
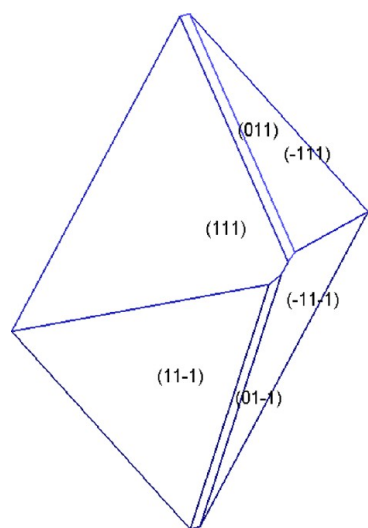

Figure 10. Wulff morphology of a CuO particle determined from calculated surface energies.

Fermi level, as shown in Figure 7. Magnetic moments of the surface copper atoms, Cu_{SUF}, are reduced to 0.59 μ_B. Oxygen atoms in the second and third layers gain small values of ~0.14

μ_B but cancel because of opposite directions. However, the top surface oxygens, O_{SUF3} and O_{SUF4}, gain positive magnetic moments of 0.17 μ_B.

CuO(010) Surface. We have investigated two possible nonpolar terminations, (010):O and (010):Cu, for the (010) surface, as shown in Figure 8 (unrelaxed structure is given in Figure S4). The (010):O terminated surface is the same as reported by Hu et al.,[63] and the surface energy for this termination is calculated to be 1.35 J/m². In this termination, oxygen atoms, O_{SUF}, in the top layer are connected to two copper atoms, Cu_{SUF1} and Cu_{SUF2}. After relaxation, the O_{SUF}–$Cu_{SUF1/2}$ bond shrinks from 1.966 to 1.846 Å (Figure 8a). These copper atoms are 3-coordinated and connected to two more oxygen atoms below, O_{SUB1} and O_{SUB2}, with bond lengths of 1.905 and 1.981 Å, respectively.

Another termination, (010):Cu, of the (010) surface is shown in Figure 8b (unrelaxed structure is given in Figure S4b), which was obtained by moving two Cu atoms from the top to the bottom of the slab. As a result, surface oxygen atoms, O_{SUF1} and O_{SUF2}, become 3-coordinated. After relaxation, we find that the top Cu atoms, Cu_{SUF}, bend to create stronger bonds with O_{SUF1} and O_{SUF2} at 1.841 and 1.821 Å, respectively. The surface energy of this termination is calculated to be 1.62 J/m² and hence less stable than (010):O termination.
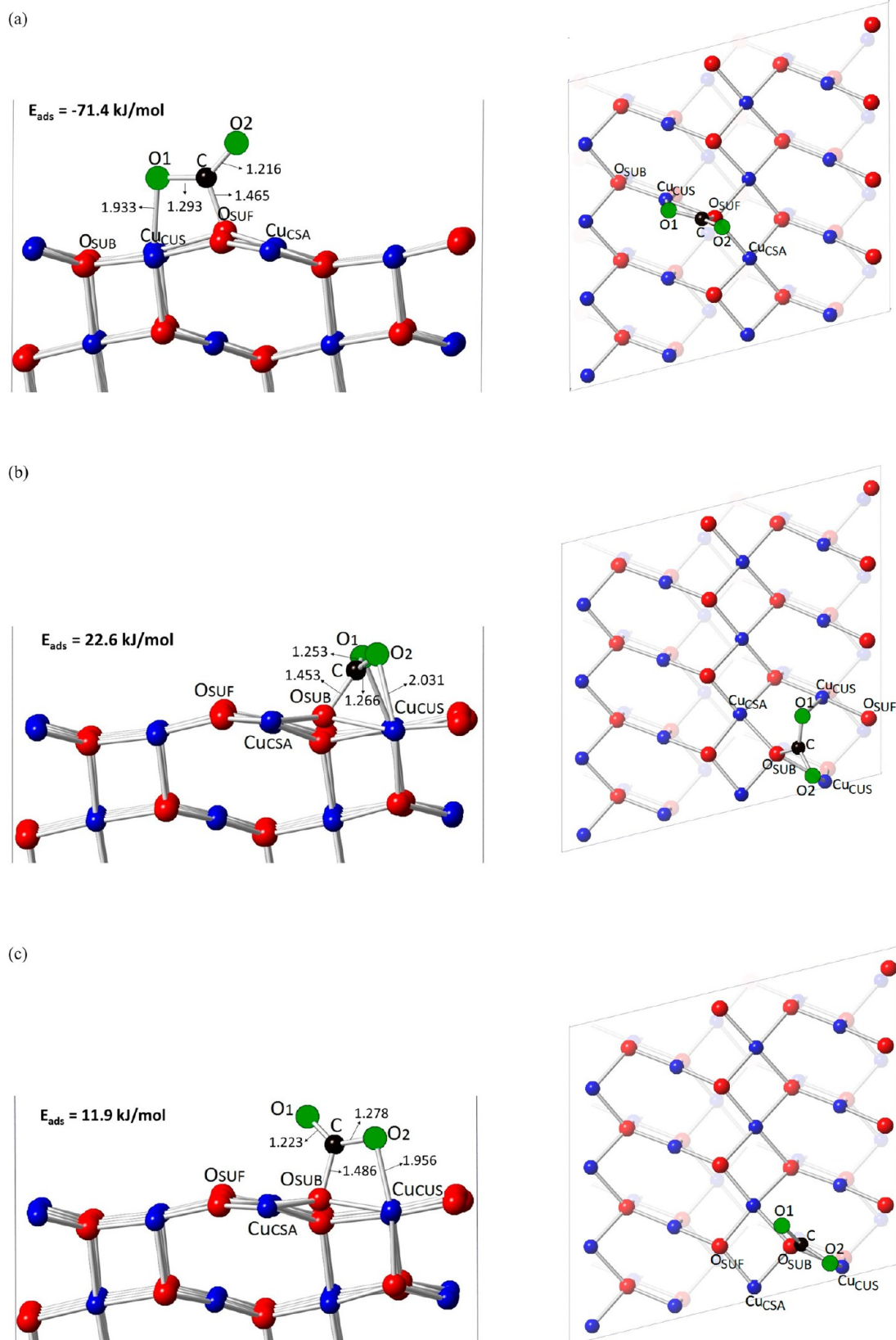
Figure 11. CO$_2$ molecule adsorbed on the CuO(111) surface in (a) configuration A, (b) configuration B, and (c) configuration C in a (2 × 2) supercell. Left panel shows the side views, while top view is shown in right panel. Blue and red color ball indicates Cu and O surface atoms, respectively, while O and C atoms of the CO$_2$ molecule are represented by green and black color balls, respectively. Bond length values are in Angstroms.

Table 4. Adsorption Energies, Representative Geometrical Parameters, Vibrational Frequencies, and Variation of the Total Bader Charge of a CO_2 Molecule Adsorbed at the (111), ($\bar{1}$11), and (011) Surfaces of CuO[a]

surface	bonding type	E_{ads}/kJ/mol	d(C–O1)/Å	d(C–O2)/Å	α(OCO)/°	d(C–O$_{SURF}$)/Å	d(O1–Cu$_{SURF}$)/Å	d(O2–Cu$_{SURF}$)/Å	ν_{as}/cm^{-1}	ν_s/cm^{-1}	ν_b/cm^{-1}	Δq(CO$_2$)/e$^-$
CO_2 (gas phase)		...	1.175	1.175	180	...	...	...	2355	1316	632	0.00
(111)	Config. A	−71.4	1.293	1.216	133.2	1.465	1.933	...	1770	1174	743	−0.15
	Config. B	22.6	1.253	1.266	131.0	1.453	2.104	2.031	...	...	...	...
	Config. C	11.9	1.223	1.278	134.4	1.486	...	1.956	...	...	...	...
($\bar{1}$11)	Config. A	−76.0	1.305	1.206	133.2	1.469	...	1.924	1807	1136	732	−0.16
	Config. B	137.5	1.278	1.265	126.1	1.422	...	2.024	...	...	...	...
(011)	Config. A	−93.2	1.280	1.244	130.8	1.420	2.025	...	1651	1219	777	−0.20
	Config. B	−54.9	1.253	1.257	132.3	1.456	2.122	2.147	...	...	...	−0.22
	Config. C	−86.5	1.276	1.239	132.7	1.445	1.982	...	...	...	...	−0.20

[a]Cu$_{SURF}$ and O$_{SURF}$ indicate the surface atoms, bonded with the CO$_2$ molecule. We have given vibrational frequencies only for the most stable exothermic configurations.

Again, bulk-like magnetic ordering is marginally preferred over line-by-line and layer-by-layer magnetic orderings as the surface energy increases by 0.16 and 0.01 J/m^2, respectively, for these two magnetic orderings in the most stable termination (010):O. We have calculated electronic DOS for this termination and found that the surface is a semiconductor with a small band gap of 0.49 eV (Figure 7). The magnetic moments of the topmost surface copper atoms, Cu$_{SUF1}$ and Cu$_{SUF2}$, have reduced to 0.63 μ_B, while all oxygen atoms are found to have zero magnetic moments.

CuO(100) Surface. The CuO(100) surface is another Tasker type III surface, and we reconstructed the surface to remove the dipole. The first reconstruction, (100):Cu, is shown in Figure 9a (unrelaxed structure is provided in Figure S5a), in which we moved one Cu atom from the top to the bottom. As a result, top oxygen atoms, O$_{SUF}$, become 3-coordinated, but after relaxation, the top Cu atoms, Cu$_{SUF}$, bend to bond to nearby surface oxygen atoms, marked as O$_{SUF3}$, with bond lengths of 2.104, 1.913, and 1.850 Å, respectively, for Cu$_{SUF}$–O$_{SUF1}$, Cu$_{SUF}$–O$_{SUF2}$, and Cu$_{SUF}$–O$_{SUF3}$ bonds, as shown in Figure 9a. The surface energy for this termination is found to be 1.83 J/m^2, and line-by-line magnetic ordering is preferred, as the surface energy increases by 0.22 and 0.05 J/m^2 for bulk-like and layer-by-layer magnetic orderings, respectively.

Another reconstruction, (100):O, leads to a more stable surface with a surface energy of 1.68 J/m^2. This surface is oxygen-terminated, and we created the nonpolar termination by moving one surface oxygen atom from the top to the bottom of the slab (Figure S5b). In the relaxed structure, the surface oxygen, O$_{SUF}$, bonds to two copper atoms, Cu$_{SUF}$ and Cu$_{SUF2}$, with bond lengths of 1.804 and 1.840 Å, respectively (Figure 9b). This surface is found to be half-metallic, having a semiconductor nature with 0.22 eV band gap for up-spin, while being a conductor for down-spin, as shown in Figure 7. We note that the magnetic moments of both surface copper atoms change: for Cu$_{SUF1}$ it reduces to 0.60 μ_B, while for Cu$_{SUF2}$ it increases to 0.70 μ_B. The magnetic moments on all oxygen atoms are found to be zero.

We derived a Wulff[46] crystal morphology of CuO (Figure 10) using the lowest surface energies for each Miller index. The three most stable surfaces (111), ($\bar{1}$11), and (011) appear in the morphology, with the (111) and ($\bar{1}$11) planes dominating the Wulff crystal shape. Other surfaces are not expressed because of their higher surface energies compared to these three surfaces. In the next section, we present our results of the CO$_2$ adsorption on the surfaces expressed in the morphology, where we have used a (2 × 2) surface supercell of CuO in order to avoid periodic interactions between neighboring units, as mentioned in Section 2.

3.3. CO$_2$ Adsorption on CuO Surfaces. *CuO(111) Surface.* We considered the most favorable, i.e., bulk magnetic ordering, for investigating the CO$_2$ adsorption on the (111) surface. As described earlier, the CuO(111) surface consists of four different atomic sites (O$_{SUF}$, O$_{SUB}$, Cu$_{SUF}$, Cu$_{SUB}$) at the top layer, and we studied the CO$_2$ adsorption by placing the molecule close to these sites parallel and perpendicularly, in different possible directions. We note that the CO$_2$ molecule moves away from the surface, when placed perpendicularly to the surface (z-direction), while it binds both exothermally and endothermally, when placed close to the O$_{SUB}$ and O$_{SUF}$ oxygen atoms, parallel to the surface (x, y-directions). The molecule also moves away from the surface when it is placed close to any of the copper atoms.
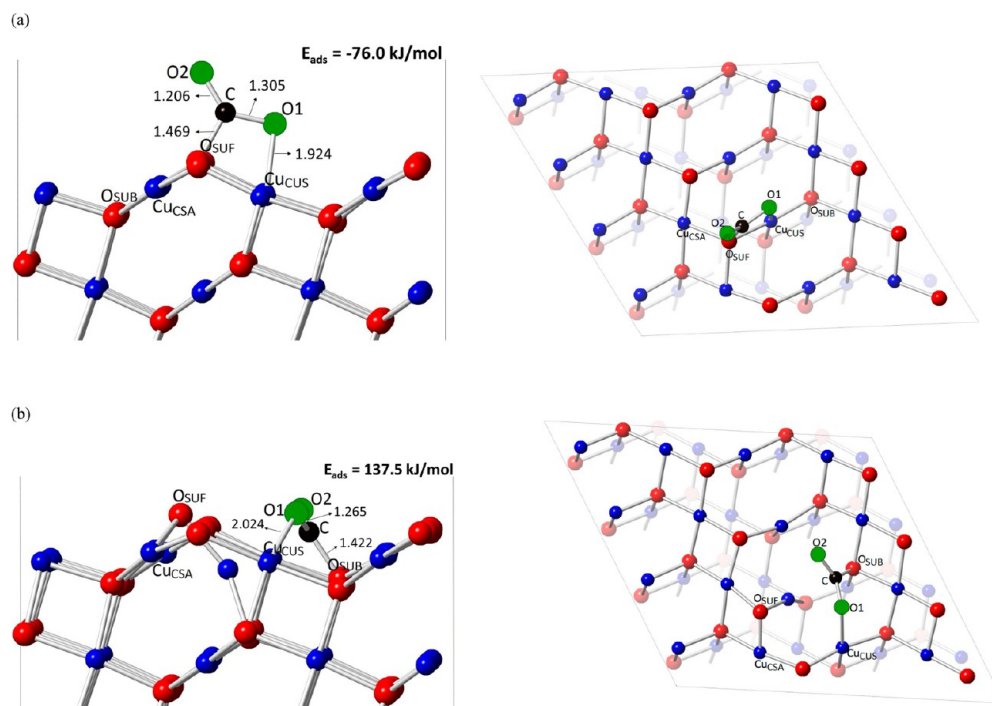
Figure 12. CO$_2$ molecule adsorbed on the CuO($\bar{1}$11) surface in (a) configuration A and (b) configuration B in a (2 × 2) supercell. Left panel shows the side views, while the top view is shown in the right panel. Blue and red color balls indicate Cu and O surface atoms, respectively, while O and C atoms of the CO$_2$ molecule are represented by green and black color balls, respectively. Bond length values are in Angstroms.

The strongest binding was found, when we placed the molecule close to the O$_{SUF}$ atom, parallel to the surface in the y-direction. This was expected as the O$_{SUF}$ atom is under-coordinated with only three Cu–O bonds. The surface oxygen, O$_{SUF}$, moves up by increasing one of the O$_{SUF}$–Cu$_{CSA}$ bond lengths from 1.966 to 2.051 Å, whereas the carbon atom, C, of the molecule bends down to bind to the O$_{SUF}$ atom ($d_{C\text{-}OSUF}$ = 1.465 Å) (Figure 11a). As a result, the CO$_2$ molecule loses its linearity with ∠OCO changing to 133.2°, whereas the C–O bonds are stretched to 1.293 and 1.216 Å for the two oxygens O1 and O2, respectively. One of the oxygen atoms, O1, binds to a surface Cu$_{CUS}$ atom, which results in an increase in the vertical distance between Cu$_{CUS}$ and an oxygen atom in the sublayer, from 1.923 to 1.933 Å. We note that in this configuration (configuration A) the CO$_2$ molecule binds exothermally to the (111) surface with an adsorption energy of −71.4 kJ/mol.

We also explored CO$_2$ interaction with the surface by placing it near O$_{SUB}$ surface atoms, both parallel (x- and y-direction) and perpendicular (z-direction) to the surface. We found that, when the CO$_2$ molecule is placed parallel to the surface in the x-direction, close to the O$_{SUB}$ atom, the O$_{SUB}$ atom moves up and breaks its bond with the Cu atom in the second layer while connecting to the C atom of the CO$_2$ molecule (Figure 11b). The CO$_2$ molecule bends to 131.0°, with its carbon atom binding to a surface O$_{SUB}$ atom with a bond length of 1.453 Å. Cu$_{CSA}$–O$_{SUB}$ and Cu$_{CUS}$–O$_{SUB}$ bond lengths also increase to about 2.5 and 10% as a result of the CO$_2$ interaction with the surface. In this configuration (configuration B), we found that the CO$_2$ molecule binds endothermally with an adsorption energy of 22.6 kJ/mol. An almost similar adsorbed geometry is found when we placed the CO$_2$ molecule close to the O$_{SUB}$ atom, parallel to the surface in the y-direction (Configuration C). Here also, the CO$_2$ molecule bends in a similar way, with

∠OCO = 134.4°, to a O$_{SUB}$ atom at a bond length of 1.485 Å (Figure 11c). The CO$_2$ adsorption is found to be endothermic with an adsorption energy of 11.9 kJ/mol. For all other initial configurations, the CO$_2$ molecule moves away from the surface. We have given the adsorption energies and parameters of the CO$_2$ adsorption geometries for all three configurations in Table 4.

CuO($\bar{1}$11) Surface. The CuO($\bar{1}$11) surface is the second-most dominant surface in the CuO morphology, and similar to the (111) surface, we explored four different atomic surface sites, Cu$_{CSA}$, Cu$_{CUS}$, O$_{SUF}$, and O$_{SUB}$, for CO$_2$ adsorption. The CO$_2$ molecule binds exothermally (E_{ads} = −76.0 kJ/mol) from all the input geometries, where the molecule is close to the Cu$_{CSA}$ and O$_{SUF}$ atoms and parallel to the surface in the x- and y-directions, respectively. In configuration A, the CO$_2$ molecule bends to bind with O$_{SUF}$ through its carbon atom (d_{C-OSUF} = 1.469 Å), and one of the oxygen O1 binds to Cu$_{CSA}$ ($d_{O1-CuCSA}$ = 1.924 Å) (Figure 12a). We note that the O$_{SUF}$ atom moves slightly upward, and the O$_{SUF}$–Cu$_{CSA}$ bond length is extended by about 10%. As a result of this molecule–surface interaction, the CO$_2$ molecule loses its linearity with ∠OCO changing to 133.2° and the C–O1 and C–O2 bond lengths elongating to 1.305 and 1.206 Å, respectively. The CO$_2$ binding in this configuration is similar to configuration A of the (111) surface.

In another configuration (configuration B), the CO$_2$ molecule binds endothermally, when placed on top of the O$_{SUB}$ atom and parallel to the surface in the x-axis direction. The molecule bends to ∼126°, with its C atom moving down to bind to an O$_{SUB}$ surface atom (d_{C-OSUB} = 1.421 Å), while one of the oxygen, O1, binds to a nearby Cu$_{CUS}$ atom (O1–Cu$_{CUS}$ = 2.024 Å). An O$_{SUB}$ atom, which was 4-coordinated earlier, breaks its bond with a Cu$_{CUS}$ atom, while the Cu$_{CUS}$ atom binds more strongly to a nearby O$_{SUF}$ atom, as shown in
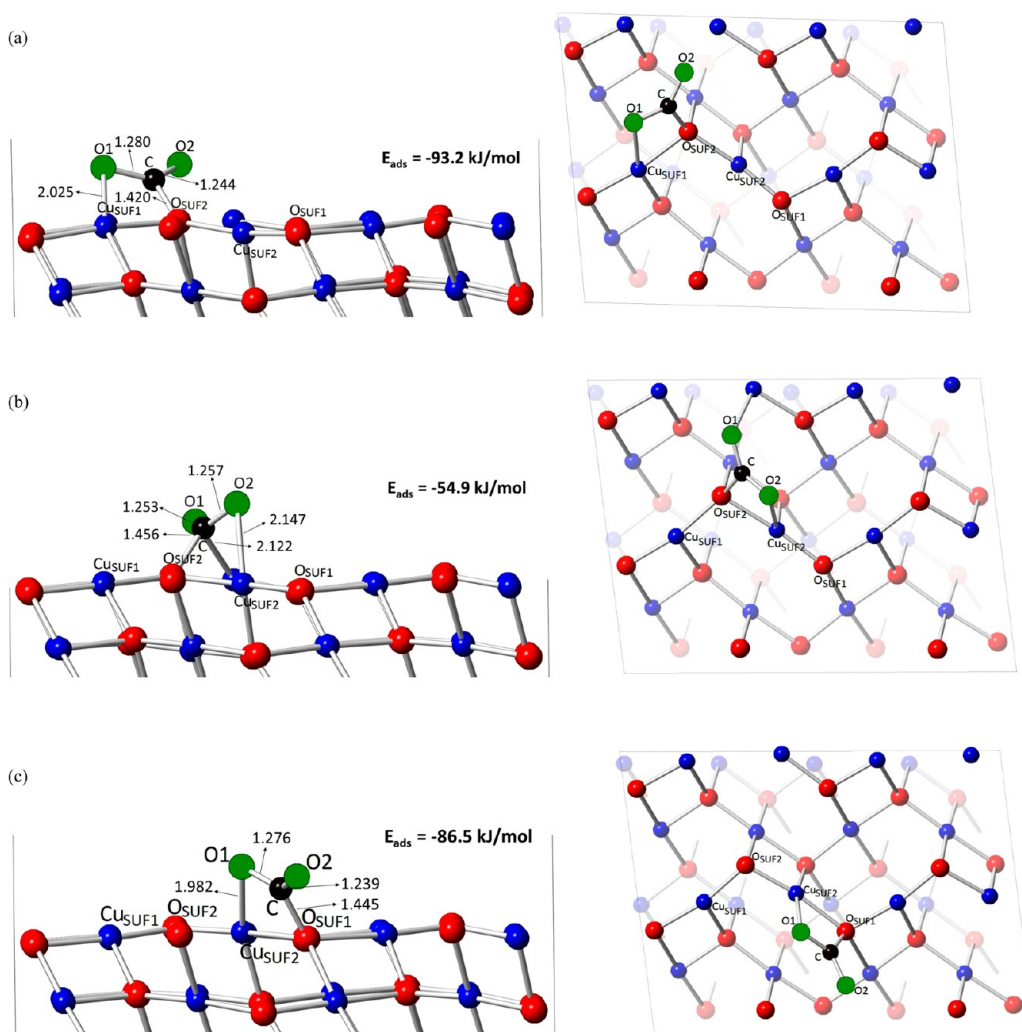
Figure 13. CO_2 molecule adsorbed on the CuO(011) surface in (a) configuration A, (b) configuration B, and (c) configuration C in a (2×2) supercell. Left panel shows the side views, while the top view is shown in the right panel. Blue and red color ball indicates Cu and O surface atoms, respectively, while O and C atoms of the CO_2 molecule are represented by green and black color balls, respectively. Bond length values are in Angstroms.

Figure 12b. However, this configuration is highly endothermic with an adsorption energy of 137.5 kJ/mol.

We note that the CO_2 molecule moves away from the surface in all configurations, where we placed the molecule near the Cu_{CSA} surface atoms. The adsorption energies and geometrical parameters of the adsorbed surface−molecule systems for A and B configurations are given in Table 4.

CuO(011) Surface. As described earlier, the CuO(011) surface consists of two oxygen (O_{SUF1}, O_{SUF2}) and two copper (Cu_{SUF1}, Cu_{SUF2}) atoms in the top layer (Figure 4c). The strongest binding is found by placing the CO_2 molecule on top of the most exposed surface oxygen atom, O_{SUF2}, parallel to the surface in the x-direction. The molecule loses linearity ($\angle OCO$ = 130.8°) and binds to the surface oxygen atom, O_{SUF2}, with a C−O_{SUF2} bond length of 1.42 Å (Figure 13a). This surface oxygen atom, O_{SUF2}, also moves upward, thereby increasing its vertical distance from the copper atom in the second layer, from 1.971 to 2.043 Å. One of the oxygen atoms, O2, of the CO_2 molecule binds to the nearby surface copper atom, with an O2−Cu bond length of 2.025 Å. We note that CO_2 binds exothermally with an adsorption energy of −93.2 kJ/mol in this configuration (configuration A).

The CO_2 molecule also binds to the surface in a different configuration (configuration B), when placed on top of the most exposed surface oxygen atom (O_{SUF2}), parallel to the surface in the y-direction. Here also, CO_2 bends when its carbon atom interacts with surface oxygen O_{SUF2}, which moves upward to form a C−O_{SUF2} bond ($d_{C-OSUF2}$ = 1.456 Å). Both oxygen atoms O1 and O2 bind at 2.147 and 2.122 Å with nearby available top surface copper atoms (Figure 13b). As a result of the interaction with the surface, the CO_2 molecule loses linearity to change $\angle OCO$ to 132.3°, and the two C−O bonds are elongated to 1.257 and 1.253 Å. In this configuration (configuration B), CO_2 adsorbs exothermally with a binding energy of −54.9 kJ/mol.

We have also explored the other surface oxygen atom (O_{SUF1}), which is comparatively less exposed, and observed that placing the CO_2 molecule parallel to the x- as well as y-directions results in another configuration, C, where this surface oxygen, O_{SUF1}, moves up and the CO_2 molecule bends to form a O_{SUF1}−C bond ($d_{OSUF1−C}$ = 1.445 Å), similar to configurations A and B. The CO_2 molecule bends to 132.7°, and one of the oxygens binds to a surface copper atom at 1.982 Å (Figure 13c). As mentioned, the O_{SUF1} atom moves up,

CuO(111)

CuO($\bar{1}$11)

CuO(011)
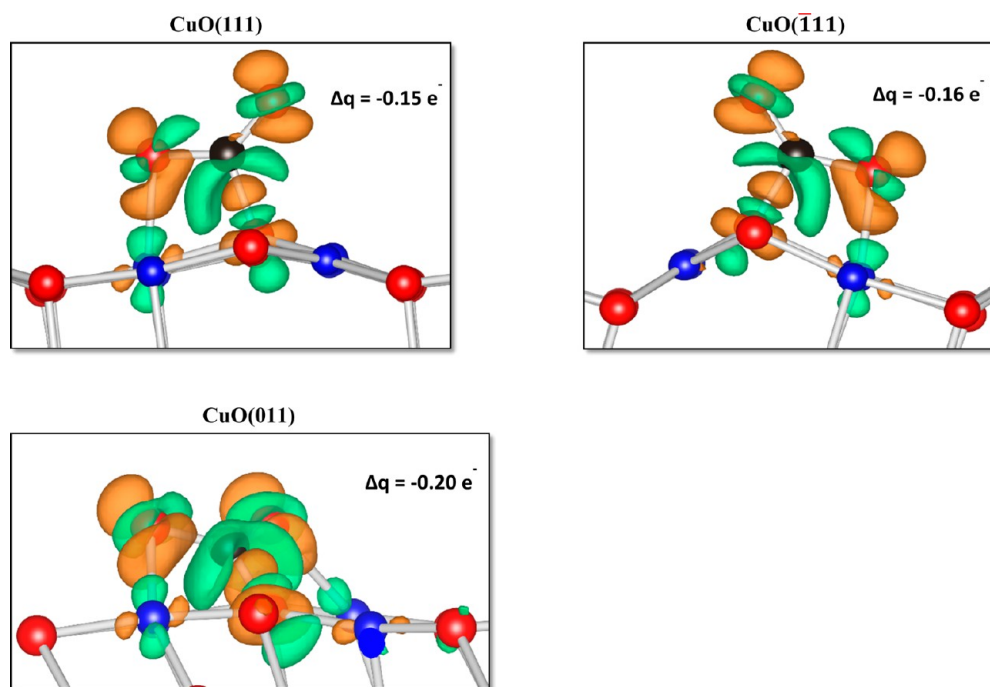
Figure 14. Electronic density difference plot of CO_2 adsorption structures on CuO (111), ($\bar{1}$11), and (011) surfaces in the most stable exothermic configurations, showing charge transfer in the regions between the CO_2 and the surface atoms upon adsorption. Orange contours indicate the electron density increases by 0.01 electrons/$\AA^3$, and green contours indicate the electron density decreases by 0.01 electrons/$\AA^3$.

increasing its bond length to the Cu atom in the second layer from 1.990 Å to 2.140 Å. Here also, the CO_2 molecule adsorbs exothermically with an adsorption energy of −86.5 kJ/mol. For all other initial configurations, where we placed the CO_2 molecule close to surface copper atoms, the molecule does not bind but moves away from the surface.

Electronic and Vibrational Analyses. We have performed Bader charge analyses of the CuO−CO_2 exothermic configurations on all three surfaces in order to quantify the electron transfer from the surface to the CO_2 molecule. From the variation of the charges on the CO_2 molecule ($\Delta q(CO_2)$) in the adsorption configurations of the different surfaces (Table 4), we observe clear charge transfer from the surface to the CO_2 molecule. We note that in the CuO(111) and ($\bar{1}$11) surfaces a net charge of ~0.15 e^- is transferred to the CO_2, while in the (011) surface, it is more prominent with a total 0.20 e^- charge transfer from the CuO surface to the adsorbed CO_2 molecule in the most stable configuration A, which again reflects stronger binding on this surface. For the other two CO_2 adsorption configurations, B and C, we note a charge transfer of 0.22 e^- and 0.20 e^-, respectively, from the (011) surface to the CO_2 molecule. In order to derive further insight into local charge rearrangement of the surfaces due to the CO_2 adsorption, we plotted the electronic charge density difference, obtained by subtracting from the charge density of the total adsorbate–substrate system, the sum of the charge densities of the CO_2 molecule, and the clean CuO surface, calculated using the same geometry as the adsorbate–substrate system. The electron density difference isosurface plots (Figure 14) show the electron redistribution within the system. We observe that as a result of CO_2 activation a net negative charge is localized on the oxygen atoms.

As noted, we observed a significant structural change in the CO_2 molecule as a result of its activation, changing from a neutral linear molecule to a negatively charged ($CO_2^{-\delta}$) bent species, with elongated C−O bond distances (Table 4). In order to further elucidate the activation, we calculated the vibrational frequencies of the adsorbed CO_2 geometry on the different surfaces for the most stable exothermic configurations. The stretched C−O bonds are confirmed by the calculated vibrational frequencies presented in Table 4. We note a significant red-shift in the C−O symmetric (v_s) and asymmetric (v_{as}) stretching modes relative to the linear gas-phase molecule, indicating that the CO_2 molecule is considerably activated. Again, the changes in the vibrational frequencies for the three surfaces are consistent with their strength of CO_2 activation, with the (011) surface exhibiting the highest red shift.

5. CONCLUSIONS

We have used DFT+U methodology to describe both bulk CuO and Cu_2O, where the U parameter was varied systematically in the range 0−9 eV in 1 eV intervals to determine the structural parameters, magnetic moment (m_s), and band gap (E_g) of CuO. The U value of 7 eV gives a very good match with the experimental literature values of the magnetic moment and band gap for CuO, while further increases result in deviation from the experimental range of these parameters. While both DFT and DFT+U fail to accurately describe the electronic structure of Cu_2O, $U = 7$ eV gives a good match with its lattice constant and other structural parameters, and employing this U correction, we have modeled different low-index surfaces of CuO. Reconstructed Tasker type III CuO(110), (010), and (100) surfaces are described in detail, and the stability of different surfaces is discussed in terms of magnetic ordering. The calculated morphology of the CuO crystal was found to be dominated by (111) and ($\bar{1}$11) surfaces, while the third most stable surface, (011), also appears in the Wulff crystal shape.

We have performed analyses of the geometries, electronic and vibrational properties of CO_2 adsorption on the three most

stable, (111), ($\bar{1}$11), and (011), surfaces of CuO, with a correction for the long-range dispersion interactions. We found that the energetically most stable (111) surface shows comparatively weak binding (~−71 kJ/mol), compared to the (011) surface, which exhibits stronger adsorption (~−93 kJ/mol). We note that the CO_2 molecule accepts electrons into its lowest unoccupied molecular orbital to form a negatively charged bent species on the surfaces. Elongation of the C−O bonds was observed in the adsorbed molecule on these surfaces compared to the gas-phase molecule, and the activation of the CO_2 molecule was confirmed via vibrational frequency analysis. Future work will include investigations of reaction pathways for the CO_2 conversion on the different surfaces of CuO.

■ ASSOCIATED CONTENT

Ⓢ Supporting Information

The Supporting Information is available free of charge on the ACS Publications website at DOI: 10.1021/acs.jpcc.5b10431.

> The density of states of Cu_2O (Figure S1), the structure of three possible magnetic orderings in CuO surfaces (Figure S2), and unrelaxed structures of the CuO (110), (010), and (100) surfaces (as Figures S3, S4, and S5, respectively) are given (PDF)

■ AUTHOR INFORMATION

Corresponding Authors
*E-mail: mishra_lu@hotmail.com, abhishek.mishra@ucl.ac.uk (akm).
*E-mail: deleeuwn@cardiff.ac.uk (nhdl).

Notes
The authors declare no competing financial interest.

■ ACKNOWLEDGMENTS

■ REFERENCES

(1) Burda, C.; Chen, X.; Narayanan, R.; El-Sayed, M. A. Chemistry and Properties of Nanocrystals of Different Shapes. *Chem. Rev.* **2005**, *105*, 1025−1102.

(2) Cava, R. J. Structural Chemistry and the Local Charge Picture of Copper Oxide Superconductors. *Science* **1990**, *247*, 656−662.

(3) Tranquada, J. M.; Sternlieb, B. J.; Axe, J. D.; Nakamura, Y.; Uchida, S. Evidence for Stripe Correlations of Spins and Holes in Copper Oxide Superconductors. *Nature* **1995**, *375*, 561−563.

(4) Liu, J.; Jin, J.; Deng, Z.; Huang, S. Z.; Hu, Z. Y.; Wang, L.; Wang, C.; Chen, L. H.; Li, Y.; Tendeloo, G. V.; Su, B. L. Tailoring CuO nanostructures for enhanced photocatalytic property. *J. Colloid Interface Sci.* **2012**, *384*, 1−9.

(5) Rossi, C.; Zhang, K.; Esteve, D.; Alphonse, P.; Tailhades, P.; Vahlas, C. Nanoenergetic Materials for MEMS: A Review. *J. Microelectromech. Syst.* **2007**, *16*, 919−931.

(6) Zhang, X.; Shi, W.; Zhu, J.; Kharistal, D. J.; Zhao, W.; Lalia, B. S.; Hng, H. H.; Yan, Q. High-power and High-energy-density Flexible Pseudocapacitor Electrodes Made from Porous CuO Nanobelts and Single-walled Carbon Nanotubes. *ACS Nano* **2011**, *5*, 2013−2019.

(7) Chen, L. B.; Lu, N.; Xu, C. M.; Yu, H. C.; Wang, T. H. Electrochemical Performance of Polycrystalline CuO Nanowires as Anode Material for Li Ion Batteries. *Electrochim. Acta* **2009**, *54*, 4198−4201.

(8) Aslani, A.; Oroojpour, V. CO Gas Sensing of CuO Nanostructures, Synthesized by an Assisted Solvothermal Wet Chemical Route. *Phys. B* **2011**, *406*, 144−149.

(9) Ali, I. New Generation Adsorbents for Water Treatment. *Chem. Rev.* **2012**, *112*, 5073−5091.

(10) Kumar, R.; Diamant, Y.; Gedanken, A. Sonochemical Synthesis and Characterization of Nanometer-Size Transition Metal Oxides from Metal Acetates. *Chem. Mater.* **2000**, *12*, 2301−2305.

(11) Wang, S. B.; Hsiao, C. H.; Chang, S. J.; Lam, K. T.; Wen, K. H.; Hung, S. C.; Young, S. J.; Huang, B. R. A CuO Nanowire Infrared Photodetector. *Sens. Actuators, A* **2011**, *171*, 207−211.

(12) Jiang, Y.; Decker, S.; Mohs, C.; Klabunde, K. J. Catalytic Solid State Reactions on the Surface of Nanoscale Metal Oxide Particles. *J. Catal.* **1998**, *180*, 24−35.

(13) Liang, X.; Gao, L.; Yang, S.; Sun, J. Facile Synthesis and Shape Evolution of Single-Crystal Cuprous Oxide. *Adv. Mater.* **2009**, *2*, 2068−2071.

(14) Huaman, R. N. E.; Jun, T. X. Energy Related CO_2 Emissions and the Progress on CCS Projects: A Review. *Renewable Sustainable Energy Rev.* **2014**, *31*, 368−385.

(15) Yin, G.; Nishikawa, M.; Nosaka, Y.; Srinivasan, N.; Atarashi, D.; Sakai, E.; Miyauchi, M. Photocatalytic Carbon Dioxide Reduction by Copper Oxide Nanocluster-grafted Niobate Nanosheets. *ACS Nano* **2015**, *9*, 2111−2119.

(16) Le, M.; Ren, M.; Zhang, Z.; Sprunger, P. T.; Kurtz, R. L.; Flake, J. C. Electrochemical Reduction of CO_2 to CH_3OH at Copper Oxide Surfaces. *J. Electrochem. Soc.* **2011**, *158*, E45−E49.

(17) Sen, S.; Liu, D.; Tayhas, G.; Palmore, R. Electrochemical Reduction of CO_2 at Copper Nanofoams. *ACS Catal.* **2014**, *4*, 3091−3095.

(18) Rajeshwar, K.; de Tacconi, N. R.; Ghadimkhani, G.; Chanmanee, W.; Janáky, C. Tailoring Copper Oxide Semiconductor Nanorod Arrays for Photoelectrochemical Reduction of Carbon Dioxide to Methanol. *ChemPhysChem* **2013**, *14*, 2251−2259.

(19) Ghadimkhani, G.; Tacconi, N. R. de; Chanmanee, W.; Janaky, C.; Rajeshwar, K. Efficient Solar Photoelectrosynthesis of Methanol from Carbon Dioxide Using Hybrid CuO−Cu_2O Semiconductor Nanorod Arrays. *Chem. Commun.* **2013**, *49*, 1297−1299.

(20) Kulik, H. J.; Wong, S. E.; Baker, S. E.; Valdez, C. A.; Satcher, J. H., Jr; Aines, R. D.; Lightstone, F. C. Developing An Approach For First-Principles Catalyst Design: Application to Carbon-Capture Catalysis. *Acta Crystallogr., Sect. C: Struct. Chem.* **2014**, *70*, 123−131.

(21) Cheng, D.; Negreiros, F. R.; Apra, E.; Fortunelli, A. Computational Approaches to the Chemical Conversion of Carbon Dioxide. *ChemSusChem* **2013**, *6*, 944−965.

(22) Wang, L.; Maxish, T.; Ceder, G. Oxidation Energies of Transition Metal Oxides within the GGA+U Framework. *Phys. Rev. B: Condens. Matter Mater. Phys.* **2006**, *73*, 195107−195113.

(23) Kohn, W.; Sham, L. D. Self-Consistent Equations Including Exchange and Correlation Effects. *Phys. Rev.* **1965**, *140*, A1133−A1138.

(24) Perdew, J. P.; Burke, K.; Ernzerhof, M. Generalized Gradient Approximation Made Simple. *Phys. Rev. Lett.* **1996**, *77*, 3865−3868.

(25) Perdew, J. P.; Zunger, A. Self-interaction Correction to Density-Functional Approximations for Many-Electron Systems. *Phys. Rev. B: Condens. Matter Mater. Phys.* **1981**, *23*, 5048−5079.

(26) Hedin, L. New Method for Calculating the One-Particle Green's Function with Application to the Electron-Gas Problem. *Phys. Rev.* **1965**, *139*, A796−A823.

(27) Svane, A.; Gunnarsson, O. Transition-Metal Oxides in the Self-Interaction−Corrected Density-Functional Formalism. *Phys. Rev. Lett.* **1990**, *65*, 1148−1151.

(28) Takahashi, M.; Igarashi, J. I. Electronic Excitations in Cupric Oxide. *Phys. Rev. B: Condens. Matter Mater. Phys.* **1997**, *56*, 12818−12824.

(29) Dudarev, S. L.; Botton, G. A.; Savrasov, S. Y.; Humphreys, C. J.; Sutton, A. P. Electron-Energy-Loss Spectra and the Structural Stability of Nickel Oxide: An LSDA+U Study. *Phys. Rev. B: Condens. Matter Mater. Phys.* **1998**, *57*, 1505−1509.

(30) Nolan, M.; Elliott, S. D. The p-type Conduction Mechanism in Cu_2O: A First Principles Study. *Phys. Chem. Chem. Phys.* **2006**, *8*, 5350−5358.

(31) Ekuma, C. E.; Anisimov, V. I.; Moreno, J.; Jarrell, M. Electronic Structure and Spectra of CuO. *Eur. Phys. J. B* **2014**, *87*, 40949−40955.

(32) Scanlon, D. O.; Morgan, B. J.; Watson, G. W. Modeling the Polaronic Nature of p-type Defects in Cu_2O: The Failure of GGA and GGA+ U. *J. Chem. Phys.* **2009**, *131*, 124703−124710.

(33) Yang, M.; He, J. Fine Tuning of the Morphology of Copper Oxide Nanostructures and Their Application in Ambient Degradation of Methylene Blue. *J. Colloid Interface Sci.* **2011**, *355*, 15−22.

(34) Chen, D. S.; Yu, W. B.; Deng, Z.; Liu, J.; Jin, J.; Li, Y.; Wu, M.; Chena, L. H.; Su, B. L. Hollow Cu_2O Microspheres with Two Active {111} and {110} Facets for Highly Selective Adsorption and Photodegradation of Anionic dye. *RSC Adv.* **2015**, *5*, 55520−55526.

(35) Lupan, O.; Cretu, V.; Postica, V.; Ababii, N.; Polonskyi, O.; Kaidas, V.; Schütt, F.; Mishra, Y. K.; Monaico, E.; Tiginyanu, I.; et al. Enhanced Ethanol Vapour Sensing Performances of Copper Oxide Nanocrystals with Mixed Phases. *Sens. Actuators, B* **2016**, *224*, 434−448.

(36) Nørskov, J. K.; Bligaard, T.; Rossmeisl, J.; Christensen, C. H. Towards the Computational Design of Solid Catalysts. *Nat. Chem.* **2009**, *1*, 37−46.

(37) Kresse, G.; Hafner, J. Ab Initio Molecular Dynamics for Liquid Metals. *Phys. Rev. B: Condens. Matter Mater. Phys.* **1993**, *47*, 558−561.

(38) Kresse, G.; Hafner, J. Ab Initio Molecular-Dynamics Simulation of the Liquid-Metal−Amorphous-Semiconductor Transition in Germanium. *Phys. Rev. B: Condens. Matter Mater. Phys.* **1994**, *49*, 14251−14269.

(39) Kresse, G.; Furthmüller, J. Efficiency of Ab-Initio Total Energy Calculations for Metals and Semiconductors Using a Plane-Wave Basis Set. *Comput. Mater. Sci.* **1996**, *6*, 15−50.

(40) Kresse, G.; Furthmüller, J. Efficient Iterative Schemes for Ab Initio Total-Energy Calculations Using a Plane-Wave Basis Set. *Phys. Rev. B: Condens. Matter Mater. Phys.* **1996**, *54*, 11169−11186.

(41) Perdew, J. P.; Burke, K.; Ernzerhof, M. Generalized Gradient Approximation Made Simple. *Phys. Rev. Lett.* **1997**, *78*, 1396.

(42) Monkhorst, H. J.; Pack, J. D. Special Points for Brillouin-Zone Integrations. *Phys. Rev. B* **1976**, *13*, 5188−5192.

(43) Henkelman, G.; Arnaldsson, A.; Jonsson, H. A Fast and Robust Algorithm for Bader Decomposition of Charge Density. *Comput. Mater. Sci.* **2006**, *36*, 354−360.

(44) Bader, R. F.W. *Atoms in Molecules: A Quantum Theory*; Oxford University Press: London, 1994.

(45) Watson, G. W.; Kelsey, E. T.; de Leeuw, N. H.; Harris, J. D.; Parker, S. C. Atomistic Simulation of Dislocations, Surfaces and Interfaces in MgO. *J. Chem. Soc., Faraday Trans.* **1996**, *92*, 433−438.

(46) Wulff, G. Zur frage der Geschwindigkeit des Wachstums und der Auflosung der Krystal-flachen. *Z. Kristallogr. - Cryst. Mater.* **1901**, *34*, 449−530.

(47) Grimme, S. Semiempirical GGA-type Density Functional Constructed with a Long-Range Dispersion Correction. *J. Comput. Chem.* **2006**, *27*, 1787−1799.

(48) Kittel, C. *Introduction to Solid State Physics*; Wiley: New York, 1976.

(49) Baumeister, P. W. Optical Absorption of Cuprous Oxide. *Phys. Rev.* **1961**, *121*, 359−362.

(50) Ghijsen, J.; Tjeng, L.; Elp, J. V.; Eskes, H.; Westerink, J.; Sawatzky, G.; Czyzyk, M. Electronic Structure of Cu_2O and CuO. *Phys. Rev. B: Condens. Matter Mater. Phys.* **1988**, *38*, 11322−11330.

(51) Chaudhary, Y. S.; Agrawal, A.; Shrivastav, R.; Satsangi, V. R.; Dass, S. A Study on the Photoelectrochemical Properties of Copper Oxide Thin Films. *Int. J. Hydrogen Energy* **2004**, *29*, 131−134.

(52) Koffyberg, F. P.; Benko, F. A. A Photoelectrochemical Determination of the Position of the Conduction and Valence Band Edges of p-type CuO. *J. Appl. Phys.* **1982**, *53*, 1173−1177.

(53) Marabelli, F.; Parravicini, G.; Salghetti, D. F. Optical Gap of CuO. *Phys. Rev. B: Condens. Matter Mater. Phys.* **1995**, *52*, 1433−1436.

(54) Wells, A. F. *Strucural Inorganic Chemistry*, 5th ed.; Clarendon: Oxford, 1984.

(55) Åsbrink, S.; Norrby, L. J. A Refinement of the Crystal Structure of Copper(II) Oxide with a Discussion of Some Exceptional e.s.d.'s. *Acta Crystallogr., Sect. B: Struct. Crystallogr. Cryst. Chem.* **1970**, *26*, 8−15.

(56) Forsyth, J. B.; Brown, P. J.; Wanklyn, B. M. Magnetism in Cupric Oxide. *J. Phys. C: Solid State Phys.* **1988**, *21*, 2917−2929.

(57) Yang, B. X.; Tranquada, J. M.; Shirane, G. Neutron Scattering Studies of the Magnetic Structure of Cupric Oxide. *Phys. Rev. B: Condens. Matter Mater. Phys.* **1988**, *38*, 174−178.

(58) Yang, B. X.; Thurston, T. R.; Tranquada, J. M.; Shirane, G. Magnetic Neutron Scattering Study of Single-Crystal Cupric Oxide. *Phys. Rev. B: Condens. Matter Mater. Phys.* **1989**, *39*, 4343−4349.

(59) Werner, A.; Hochheimer, H. D. High-Pressure X-Ray Study of Cu_2O and Ag_2O. *Phys. Rev. B: Condens. Matter Mater. Phys.* **1982**, *25*, 5929−5934.

(60) Isseroff, L. Y.; Carter, E. A. Importance of Reference Hamiltonians Containing Exact Exchange for Accurate One-Shot GW Calculations of Cu_2O. *Phys. Rev. B: Condens. Matter Mater. Phys.* **2012**, *85*, 235142−235148.

(61) Tasker, P. W. The Stability of Ionic Crystal Surfaces. *J. Phys. C: Solid State Phys.* **1979**, *12*, 4977−4984.

(62) Bowker, M.; Stone, P.; Smith, R.; Fourre, E.; Ishii, M.; Leeuw, N. H. de. The Surface Structure of BaO on Pt(111):(2 × 2)-Reconstructed BaO(111). *Surf. Sci.* **2006**, *600*, 1973−1981.

(63) Hu, J.; Li, D.; Lu, J. G.; Wu, R. Effects on Electronic Properties of Molecule Adsorption on CuO Surfaces and Nanowires. *J. Phys. Chem. C* **2010**, *114*, 17120−17126.

(64) Koffyberg, F. P.; Benko, F. A. A Photoelectrochemical Determination of the Position of the Conduction and Valence Band Edges of p-type CuO. *J. Appl. Phys.* **1982**, *53*, 1173−1177.